Safe targeting of T cell acute lymphoblastic leukemia by pathology specific NOTCH inhibition

Roger A. Habets[1,2#], Charles E. de Bock[3,4,5#], Lutgarde Serneels[1,2], Inge Lodewijkx[3,4], Delphine Verbeke[3,4], David Nittner[6,7] Rajeshwar Narlawar[1], Sofie Demeyer[3,4], James Dooley[2,8], Adrian Liston[2,8], Tom Taghon[9,10], Jan Cools[3,4,*] and Bart de Strooper[1,2,11,*]

[1] Department of Neurosciences, Leuven Institute for Neuroscience and Disease, (LIND), KU Leuven, Leuven, Belgium

[2] VIB Center for Brain and Disease Research, VIB, Leuven, Belgium

[3] Center for Human Genetics, KU Leuven, Leuven, Belgium

[4] VIB Center for Cancer Biology, VIB, Leuven, Belgium

[5] Children's Cancer Institute, Lowy Cancer Research Centre, UNSW, Sydney, NSW 2052, Australia

[6] Histopathology Expertise Center, VIB-KU Leuven Center for Cancer Biology, Leuven, Belgium

[7] Department of Oncology, KU Leuven, Leuven, Belgium

[8] Department of Microbiology and Immunology, KU Leuven, Leuven, Belgium

[9] Department of Clinical Chemistry, Microbiology and Immunology, Ghent University, Ghent, Belgium

[10] Cancer Research Institute Ghent, Ghent, Belgium

[11] Dementia Research Institute, University College London, London, UK

[#] These authors contributed equally to this work as co-first authors

[*] **Corresponding authors:** bart.destrooper@kuleuven.vib.be or jan.cools@kuleuven.vib.be

Abstract

Given the high frequency of activating *NOTCH1* mutations, inhibition of the γ-secretase complex remains an attractive target for T cell acute lymphoblastic leukemia (T-ALL). However, available inhibitors block all four existing γ-secretase complexes equally and lead to severe "on-target" gastrointestinal tract, skin and thymus toxicity, limiting their therapeutic applications. Here, we demonstrate that genetic deletion or pharmacologic inhibition of Presenilin-1 is highly effective in decreasing leukemia whilst avoiding dose-limiting toxicities. Therefore, Presenilin-1 selective compounds provide a new therapeutic strategy for safe and effective targeting of T-ALL and should be considered for other diseases in which NOTCH signaling plays a role.

One Sentence Summary

Selective inhibition of Presenilin-1 γ-secretase complexes efficiently targets T cell acute lymphoblastic leukemia whilst overcoming dose-limiting side-effects observed with complete γ-secretase inhibition.

Introduction

γ-Secretases are a group of widely expressed, intramembrane-cleaving proteases. The enzymes process clinical relevant substrates such as APP and NOTCH and have been explored as drug targets in Alzheimer's disease, cancer and other disorders *(1)*. However, the clinical use of γ-secretase inhibitors (GSIs) has been hampered due to severe mechanism-based dose-limiting toxicity; predominantly intestinal goblet cell hyperplasia and concomitant severe diarrhea *(2)*, thymus atrophy and ablated T cell development *(3, 4)*, splenic marginal zone atrophy *(5)* and skin lesions *(6)*. This toxicity is due to systemic NOTCH inhibition because NOTCH receptors require γ-secretase complex-mediated processing for the release and nuclear translocation of the NOTCH intracellular domain (NICD) in order to activate gene expression *(7)*.

It is, however, important to realize that the enzymatic activity of the γ-secretase complex reflects the combined activity of at least four different complexes. Clinical trials have been performed with broad-spectrum, non-selective γ-secretase inhibitors that target all four complexes equally. The question remains whether inhibition of some but not all γ-secretase complexes, by subunit selective targeting, could provide a way forward to safe targeting.

The four different γ-secretase complexes each contain one Nicastrin (NCSTN) and one Presenilin enhancer 2 (PEN-2) subunit. In addition, two different APH-1 proteins, APH-1A or APH-1B, and two different Presenilin (PSEN) proteins, PSEN1 or PSEN2, exist. One of the APH-1 and one of the PSEN proteins combine with the two stable subunits to generate four different subcomplexes, which differ in their PSEN subunit and/or APH-1 subunit *(8, 9)*. Different γ-secretase complexes can be expressed simultaneously by the same cells and at the same time *(1, 10)*, but differ in their subcellular distribution and their biological function *(11-13)*. Indeed, gene targeting of the different complexes revealed a variety of different outcomes, going from very severe embryonic lethal Notch phenotypes *(7, 14-16)*, over subtle behavioral phenotypes *(17, 18)*, to even normal mice *(19)*.

The γ-secretase complexes have been mainly investigated in the context of Alzheimer's Disease as they process the Amyloid Precursor Protein (APP) to generate different amyloid-β profiles *(12)*. Besides, γ-secretase inhibitors have been actively investigated as targeted therapeutics for T cell acute lymphoblastic leukemia (T-ALL) *(20)*, an aggressive hematologic malignancy resulting from the transformation of immature T cell progenitors *(21, 22)*. In T-ALL, activating *NOTCH1* mutations are the most common mutations observed, present in approximately 60% of all cases *(23-25)*. These mutations result in increased and ligand-independent oncogenic NOTCH1 signaling, promoting T cell transformation through the physiologic functions of NOTCH1 in the thymus *(24, 26)*. However, like physiologic NOTCH1 signaling, oncogenic mutant NOTCH1 signaling still requires γ-secretase processing for activation, providing the strong rationale for GSIs as a therapeutic approach for T-ALL *(20, 27-29)*.

Next to T-ALL, increasing evidence is supporting a causative role for NOTCH gain-of-function mutations in solid cancers. These tumors often display inappropriate NOTCH signaling due to overexpression of NOTCH receptors and/or ligands or loss of negative regulation of NOTCH signaling *(30)*. Because of this, γ-secretase inhibitors were also investigated for a number of hematological and solid cancers, including breast cancer, pancreatic cancer, glioma, non-small cell lung cancer and colorectal cancer. However, despite extensive research to develop several classes of GSIs, none did spare physiologic NOTCH signaling sufficiently and none of these drugs was successful in clinical trials. This has led to a halt for the therapeutic development of γ-secretase inhibitors in these areas. The hypothesis that selective inhibition of one of the γ-secretase complexes alone, targeting the enzyme most active in the tumors while sparing other γ-secretase complexes in the hope to preserve physiological Notch signaling in the healthy tissues, has not been tested, however.

Here, we wanted to address whether selective γ-secretase inhibition could be a valid therapeutic approach. Given the high frequency of *NOTCH1* mutations in T-ALL that result in ligand-independent, but γ-secretase dependent signaling, T-ALL provides a perfect model to evaluate this hypothesis. We selectively targeted the PSEN1-containing γ-secretase complexes, while leaving the PSEN2-containing complexes untargeted. By doing so, we observed a strong clinical efficacy for the treatment of T-ALL without the observed toxicity inherent to broad-spectrum GSIs.

Results

Presenilin-1 is highly expressed in T-ALL and regulates NOTCH1 cleavage

The Presenilin subunits PSEN1 or PSEN2 provide the catalytic center of the different γ-secretase complexes (**Fig. 1a**). Microarray analysis revealed that both *PSEN1* and *PSEN2* are expressed during human T cell development, albeit *PSEN1* is expressed at about four-fold higher levels compared to *PSEN2* (**Fig. 1b**). *PSEN1* expression is however >30-fold higher than *PSEN2* expression in T-ALL cell lines and primary T-ALL patient samples *(31, 32)* (**Fig. 1c**). NOTCH1 signaling is essential for early T cell development in both mice and humans *(26, 33)*, therefore we examined whether Psen1 loss would abrogate normal T cell development in mice. Previously, a conditional *Psen1* knockout mouse was

generated by targeting exon 2/3 *(34)*. We developed a new conditional *Psen1* knockout mouse targeting exon 1 that also contained a Tag (*Psen1*$^{f/f}$) (**Fig. S1a**) and then crossed this with a CD2Cre transgenic mouse *(35)* to inactivate *Psen1* in developing T cells (CD2CrePsen1$^{\Delta/\Delta}$ mice). The introduction of LoxP sites and a Tag into the *Psen1* gene locus alone caused a 50% decrease in Psen1 protein expression in thymocytes, but did not result in major T cell defects (**Fig. 1d-f; Fig. S1b-d**). Notably, the complete loss of Psen1 expression in thymocytes of CD2CrePsen1$^{\Delta/\Delta}$ mice did not alter the frequency of major T cell populations in the thymus (**Fig. 1d-f)**. Although a small compensatory increase of Psen2 expression was seen after loss of Psen1, this was insufficient to overcome the overall loss in γ-secretase complex formation assessed by the strong reduction in Nicastrin maturation (**Fig. S1b,c**). To study the possible effect on T cell proliferation, we generated *ex vivo* cultures of mouse pro-T cells derived from C57BL/6 wild type, *Psen1*$^{f/f}$ or CD2Cre*Psen1*$^{\Delta/\Delta}$ mice (**Fig. S2a).** These pro-T cells are cultured on Dll4 (Notch1 ligand)-coated plates and are strictly dependent on Dll4-induced Notch signaling *(36)*. Pro-T cells derived from CD2Cre*Psen1*$^{\Delta/\Delta}$ mice showed comparable proliferation to controls (**Fig. 1g**), demonstrating that Psen1 is dispensable for normal T cell development. Apparently, the presence of Psen2 is sufficient to maintain an adequate level of Notch signaling to support normal development.

We next investigated whether *Psen1* gene inactivation could affect processing of mutant forms of the NOTCH1 receptor found in T-ALL. We transduced the mouse pro-T cells established from C57BL/6 wild type, *Psen1*$^{f/f}$ or CD2Cre*Psen1*$^{\Delta/\Delta}$ mice with a constitutively active and clinically relevant mutant NOTCH1 receptor, containing a HD and PEST domain mutation (NOTCH1-L1601P-ΔP). This mutant NOTCH1 receptor provides a substrate for γ-secretase, which is independent of ligand stimulation *(24)*. C57BL/6 wild type and Psen1$^{f/f}$ derived pro-T cells transduced with mutant NOTCH1 receptors were able to survive and proliferate in the absence of Dll4, confirming that the NOTCH1-L1601P-ΔP mutant can signal in the absence of Dll4. Interestingly, Psen1 deletion significantly reduced pro-T cell proliferation and survival of NOTCH1-L1601P-ΔP expressing cells (**Fig. 1h**) and decreased mutant NOTCH1 receptor processing and NICD1 formation (**Fig. 1i**). Taken together, these data indicate that loss of Psen1 specifically reduces oncogenic NOTCH1 signaling in T cells, whilst having limited effect on physiologic Dll4-mediated Notch signaling.

Genetic deletion of Presenilin-1 prolongs survival in NOTCH1-induced T cell leukemia in vivo

Given that loss of Psen1 perturbs the processing and downstream signaling of mutant NOTCH1 receptors involved in T-ALL, we next assessed if *Psen1* deletion could also impair mutant NOTCH1-induced T-ALL development *in vivo*. To this end, we transplanted wild type C57BL/6 mice with syngeneic wild type C57BL/6, *Psen1*$^{f/f}$ or CD2Cre*Psen1*$^{\Delta/\Delta}$ hematopoietic progenitors, expressing equivalent levels of ΔEGF-NOTCH1-L1601P-ΔP, inferred from the level of GFP expression, after retroviral transduction. (**Fig. 2a,b; Fig. S2b**). Mice transplanted with wild type or Psen1$^{f/f}$ cells transduced with ΔEGF-NOTCH1-L1601P-ΔP showed circulating GFP$^+$ CD4$^+$CD8$^+$ T cells at 6 weeks post transplantation, indicative for leukemia development (**Fig. 2c,d**). Significantly, mice transplanted with CD2Cre*Psen1*$^{\Delta/\Delta}$ cells transduced with ΔEGF-NOTCH1-L1601P-ΔP were largely devoid of circulating GFP$^+$ T cells at 6 weeks post transplantation. At 9 weeks, mice transplanted with wild type and *Psen1*$^{f/f}$ cells displayed splenomegaly and thymic enlargement due to CD4$^+$CD8$^+$ leukemic cell infiltration, which was still absent in mice transplanted with CD2Cre*Psen1*$^{\Delta/\Delta}$ cells (**Fig. 2e,f; Fig. S2c**). These differences were not due to impaired homing and engraftment following transplantation of the CD2Cre*Psen1*$^{\Delta/\Delta}$ hematopoietic progenitors (**Fig. S2d**). Eventually, only 9 out of 17 mice transplanted with CD2Cre*Psen1*$^{\Delta/\Delta}$ progenitors developed CD4$^+$CD8$^+$ leukemia, with a median overall survival of 120 days compared to 73 and 72 days median survival in wild type and *Psen1*$^{f/f}$ transplanted mice, respectively ($p<0.0001$, **Fig. 2g,h**). These data show that deficiency of Psen1 alone is sufficient to majorly affect murine T-ALL induction.

Next, we set out to elucidate whether *Psen1* loss in an already established leukemia could still impair disease progression. To this end, we generated inducible *Psen1* conditional knockouts by crossing *Psen1*$^{f/f}$ to Rosa26Cre-ER^{T2} mice, generating R26Cre-ER^{T2}Psen1$^{f/f}$ mice. C57BL/6 mice were then transplanted with R26Cre-ER^{T2}*Psen1*$^{f/f}$ hematopoietic progenitors transduced with ΔEGF-NOTCH1-L1601P-ΔP. Following successful engraftment, *Psen1* was specifically deleted in transplanted donor cells through tamoxifen treatment (100 mg/kg for 5 days). These experiments were performed in primary recipient mice and were repeated also in tertiary transplanted recipient mice to assess whether loss of

Psen1 in an aggressive leukemia setting still hampers disease progression (**Fig. 3a**). Analysis of R26Cre-ER^{T2}Psen1$^{f/f}$ leukemic cells recovered after tamoxifen treatment showed complete ablation of Psen1 (**Fig. S3a**). Specific *Psen1* deletion in the donor cells reduced leukemia burden, assessed by the fraction of circulating GFP^{+} cells in the peripheral blood, by two-fold at 5 weeks post transplantation and >6-fold at 9 weeks post transplantation in the primary recipient mice, compared to vehicle-treated mice (**Fig. 3b**). One-week post tamoxifen treatment, analysis of age-matched mice showed that *Psen1* deletion reduced splenomegaly by 50% compared to vehicle-treated mice (**Fig. 3c**). Furthermore, *Psen1* deletion by tamoxifen treatment in an established leukemia increased the median overall survival to 142 days compared to 84,5 days for vehicle-treated mice ($p<0.0001$, **Fig. 3d**). The tamoxifen treated mice that did develop leukemia had lost Psen1, excluding the possibility of having escaped recombination, but did show robust Psen2 expression (**Fig. S3b**). Importantly, tamoxifen treatment had no effect on leukemia progression and overall survival in mice transplanted with wild type C57BL/6 tumor cells expressing *Psen1* endogenously, compared to vehicle controls (**Fig. S3c**).

Finally, we tested whether *Psen1* was required for leukemia maintenance and progression by targeting *Psen1* in a more aggressive and developed leukemia. Tertiary recipients were transplanted with leukemic cells from mice that suffered from full blown leukemia and these tertiary recipients were treated with vehicle or tamoxifen. Even in this aggressive leukemia model, *Psen1* deletion had a significant effect on survival ($p<0.001$, **Fig. 3e**). Taken together, these data show the importance of Psen1 in leukemia development and maintenance and validate Psen1 as a potential target for therapy in T-ALL cases with NOTCH1 mutations.

Pharmacologic inhibition of Presenilin-1 impairs leukemia progression and prolongs survival in vivo

The significant decrease in leukemic burden identified through genetic loss of *Psen1* prompted us to investigate whether selective pharmacological PSEN1 inhibition would be a viable strategy for T-ALL treatment. To this end, we tested whether the PSEN1-selective inhibitor MRK-560, which has ~100-fold selectivity over PSEN2 *(37)* (**Fig. S4**), could block mutant NOTCH1 receptor signaling in human T-ALL cell lines. Indeed, MRK-560 treatment reduced NICD1 generation in HPB-ALL, DND-41 and

Jurkat cell lines and resulted in a dose-dependent decrease of proliferation in HPB-ALL and DND-41, which depend on NOTCH signaling for their survival (**Fig. 4a,b**). Jurkat T-ALL cells harbor a *PTEN* deletion and are not dependent on NOTCH signaling for their proliferation which explains why these cells do not show a decrease in survival upon MRK-560 treatment *(28, 38, 39)* (**Fig. 4b; Table S2**). Similar to broad-spectrum γ-secretase inhibitors, the effect of the PSEN1-selective γ-secretase inhibitor MRK-560 on proliferation could be attributed to a block in cell cycle (**Fig. 4c,d**).

Next, we determined whether pharmacological PSEN1 inhibition impaired T-ALL *in vivo*. ΔEGF-NOTCH1-L1601P-ΔP T-ALL lymphoblasts were injected into secondary recipients and treated with 30 μmol/kg MRK-560 or vehicle for 14 days. MRK-560 treatment resulted in strong anti-leukemic effects and improved median survival to 30 days compared to 18 days in vehicle-treated mice (p=0.0009, **Fig. 4e**). These data show significant therapeutic effects for pharmacological PSEN1 inhibition in *in vitro* and *in vivo* T-ALL models.

Having validated selective PSEN1 inhibition in a NOTCH1-driven mouse leukemia model, we next investigated the efficacy of PSEN1 targeting in human patient-derived xenograft (PDX) *in vivo* models. Immunodeficient NSG mice were injected with four genetically different PDX T-ALL samples with different *NOTCH1* mutations (**Table S2**). Mice were randomized into vehicle and MRK-560 treatment arms and were treated with 30 μmol/kg MRK-560 or vehicle for 14 days by subcutaneous injection. MRK-560 treatment significantly reduced leukemia burden compared to vehicle treated mice, as assessed by peripheral blood counts of human $CD45^+$ cells and *in vivo* bioluminescence (**Fig. 5a-d; Fig. S5a-b**). The various degree of response to MRK-560 treatment was not explained by differences in *PSEN1* expression in the PDX models (**Fig. S5c**).

Analysis of age-matched vehicle versus MRK-560-treated mice at the end of a 2-week treatment period showed up to 60% reduction in splenomegaly and up to 40% reduction in leukemic cell infiltration in the spleens of MRK-560 treated mice (**Fig. 5e-g**). Human HLA staining revealed a marked reduction of human leukemia cells in the spleen of MRK-560 treated animals compared to vehicle treatment, associated with reduced Ki67 staining, in line with reduced leukemia burden and inhibition of

proliferation (**Fig. S5d,e**). Most importantly, MRK-560 treatment significantly prolonged survival compared to vehicle treated mice in all three *NOTCH1* mutant T-ALL patient samples tested here (1.1 fold, p=0.0001 for 389E, 1.5 fold, p=0.0011 for XC63 and 1.6 fold, p=0.0027 for XC65; **Fig. 5h-j**). Notably, single agent MRK-560 treatment was still effective even when treatment was initiated in mice with a high leukemia burden ("curative setting"), which resembles the clinical setting where disease is only detected when blood counts start to change (**Fig. 5c,j**). In these conditions, a 1,5 fold increased survival compared to vehicle treated mice was observed (p=0.0011; **Fig. 5j**). Moreover, relapsing mice also remained sensitive to a second round of MRK-560 treatment indicating no short-term outgrowth of an overtly resistant leukemia clone (**Fig. S5F**). Analysis of leukemic cells following MRK-560 treatment showed that canonical NOTCH target genes *MYC*, *DTX1* and *NOTCH3* were downregulated in T-ALL cells from MRK-560 treated mice compared to vehicle treated mice (**Fig. 5k**), confirming "on-target" effects for MRK-560.

Pharmacological Presenilin-1 selective targeting does not cause gastrointestinal toxicity nor T cell developmental defect

The major hurdle in adopting γ-secretase inhibitors clinically has been the "on-target" NOTCH-related toxicity, resulting in severe gastrointestinal goblet cell hyperplasia or defective T cell development. Significantly, treatment with the PSEN1-selective γ-secretase inhibitor MRK-560 did not cause any pathological changes in the gastrointestinal architecture nor increased numbers of secretory goblet cells, assessed by Periodic Acid-Schiff (PAS) staining (**Fig. 6a**). In contrast, treatment with the classical broad-spectrum γ-secretase inhibitor Dibenzazepine (DBZ, 10μmol/kg) resulted in a 4-fold increase in the number of secretory goblet cells, characteristic of gastrointestinal toxicity due to systemic NOTCH inhibition, as previously reported *(2)*. Moreover, 4 week treatment of wild type mice with intermitted dosing of DBZ, as described previously *(40)*, was still more toxic compared to MRK-560 (**Fig. S6**). The expression levels of *PSEN1* and *PSEN2* within the human small intestine are nearly equivalent (**Fig. 6b**) suggesting that in the absence of PSEN1, the activity of PSEN2 may be sufficient to maintain normal gastrointestinal physiology. Furthermore, immunophenotyping revealed no major defects in thymic T cell development in healthy C57BL/6 mice treated with MRK-560 for 14 days, with cells progressing

normally into $CD4^+CD8^+$ T cells (**Fig. 6c-e**), in line with the genetics experiments shown in Figure 1. In contrast, mice treated with DBZ showed defective T cell development, displayed by a marked reduction in $CD4^+CD8^+$ T cells and an increase in DN1 stage T cells, as previously reported for classical γ-secretase inhibitors. Altogether, these data provide evidence for a clear therapeutic window for selective PSEN1 targeting in T-ALL.

Discussion

Activating *NOTCH1* mutations are found in approximately 60% of T-ALL patients and across all T-ALL subtypes *(24, 31)*. Therefore, targeting NOTCH1 by using GSIs that block NOTCH processing and activation has been of continuing clinical interest in the treatment of T-ALL. The gastrointestinal toxicity inherent to general GSIs ameliorates partially with intermittent dosing regimens; nonetheless, the most recent clinical trials were still halted prematurely due to severe adverse effects *(2, 6, 41)*. Here, we deliver proof of concept that selective targeting of PSEN1 γ-secretase complexes provides a viable and attractive alternative therapeutic approach. Both genetic and pharmacological experiments showed consistently that PSEN1 targeting alone is sufficient to strongly mitigate leukemia development, both in mutant NOTCH1-driven leukemia mouse models and in human patient-derived xenograft models. Using a tamoxifen inducible model for *Psen1* deletion, we were able to show that these effects were also observed when *Psen1* was targeted after leukemia had developed, which more closely resembles the clinical situation. Importantly, the beneficial effects of pharmacological Psen1 targeting were also observed when treatment was initiated at high blast count, which is classified clinically as higher risk with worse prognosis *(42, 43)*. These data show that selective targeting of PSEN1 γ-secretase complexes provides a potent approach displaying high anti-leukemic activity, comparable to complete γ-secretase inhibition *(44)*. These data are supported by an earlier observation that Psen1 is required for the development of a DLL4 driven T-cell lymphoma on a Psen2 null background *(45)*. While that work demonstrated that PSEN1 is necessary, it did not demonstrate that it is sufficient to inhibit Psen1 alone to block the lymphoma. Some mice in our experiments, with confirmed Psen1 deletion, still developed leukemia likely due to the observed compensatory high Psen2 expression in these cells. Therefore, although PSEN2 is not expressed in human T-ALL, reactivation of PSEN2 expression might be a

potential resistance mechanism. Interestingly, γ-secretase inhibition can reduce the frequency of leukemic stem cells, since mutant NOTCH1 signaling promotes reprogramming to these leukemic stem cells *(46-49)*. Although not tested here, our findings suggest that selective PSEN1 targeting might also have the promise to target these quiescent and therapy-resistant cells, believed to be responsible for T-ALL relapse.

Importantly, the selective pharmacological inhibition of Psen1 did not result in gastrointestinal toxicity or T cell development defects in mice, opposed to the adverse effects observed by complete γ-secretase inhibition by DBZ. Our work extends a previous study in Alzheimer's disease models where selective γ-secretase inhibition was efficacious and tolerable, although treatment periods in these studies were significantly shorter than in the current work *(37, 50)*. This lack of toxicity *in vivo* may find partial explanation in the observation that *PSEN2* and *PSEN1* expression levels are more equivalent within the gastrointestinal tract and developing T cells compared to T-ALL cells. Indeed, *Psen2*-knockout mice exposed to MRK-560 did display gastrointestinal and thymus toxicity, comparable to full γ-secretase inhibition, indicating that Psen2 is responsible for the protective effects *(37)*. So although Psen2 is insufficient to compensate for *Psen1* deletion during development *(15)*, sparing Psen2 activity maintains physiological relevant signaling in the gut and hematopoietic system during adult life. To completely proof that Psen2 activity can compensate for the lack of Psen1 activity, future studies will require a complete selective genetic knockout of *Psen1* in the gut, e.g. using a villin-Cre mouse model. However, for all practical means it is clear that a PSEN1-selective inhibition is highly preferable above the typical broad-spectrum inhibition that is induced by the previously tested γ-secretase inhibitors. Thus, in human T-ALL cells, *PSEN1* expression is significantly higher compared to *PSEN2* expression (**Fig. 1**) and *PSEN2* expression is likely too low to provide sufficient support for leukemia development. Measuring *PSEN1/2* expression levels in circulating T-ALL cells might be a helpful parameter to decide whether selective PSEN1 targeting might be beneficial. In addition, PSEN1 and PSEN2 complexes have different subcellular profiles, resulting in substrate selectivity due to differential compartmentalization *(11)*. Therefore, the differential sensitivity for leukemic cells versus normal tissue observed with the PSEN1 inhibitor might also be partially explained by enzyme-substrate specificity due to different subcellular

localization. Further work should determine whether mutant NOTCH1 is processed at the cell surface where PSEN1 complexes are predominantly expressed while wild type NOTCH1 is processed additionally in endocytic compartments, where PSEN2 complexes reside *(11)*.

Our study is conducted using preclinical experimental models that may not completely recapitulate their human counterparts. The murine leukemia models used were solely driven by mutant NOTCH1 signaling, whereas patients diagnosed with leukemia often display multiple different genetic lesions. However, the four human PDX samples used to determine the potency of pharmacological PSEN1-selective targeting displayed various mutational backgrounds, strengthening our preclinical findings. In addition, human PDX models have shown concordance between preclinical results and corresponding available clinical data *(51)*, making them a good model to study new potential therapeutic approaches. In any event, the overall increased safety profile of selective PSEN1 γ-secretase inhibition warrants optimism for further clinical development. Carefully monitoring of thymus, gastrointestinal tract, and also skin, which is known to be sensitive for tumorigenesis when *Psen1* is deleted *(6, 52)*, will be necessary when further addressing the clinical feasibility of Psen1 selective targeting in patients.

Finally, if further proof of concept can be established in T-ALL patients, even more applications for selective γ-secretase inhibition in the clinic could be envisaged. Indeed, safe selective γ-secretase inhibition might be useful as additional therapy in a variety of other cancers with deregulated NOTCH signaling, such as B-cell lymphoma, breast cancer and glioma *(53-55)*. Furthermore, clinical interest in γ-secretase inhibition might become revived in other therapeutic areas where development was stopped because of gastrointestinal side effects, such as acute hearing loss *(56, 57)*; peritoneal fibrosis as a complication of dialysis in renal disease *(58)*; and atherosclerosis *(59, 60)*.

Materials and Methods

Study design. We hypothesized that selective targeting of specific γ-secretase subunits is a safe strategy to target *NOTCH1* mutant T cell acute lymphoblastic leukemia. Cell culture experiments using cell lines

were performed at least three times. *Ex vivo* T cell cultures were performed using at least three different mice to generate pro-T cells from, unless otherwise noted. For treatment studies involving mice, disease burden was determined at treatment initiation and animals were rank-ordered and divided into treatment arms after assuring that mean disease burden was comparable among groups. For toxicity studies in mice, animals were randomly assigned to treatment groups. Sample sizes were chosen based on prior experience and power calculations of expected differences with this type of experiments. Sample sizes for *in vivo* experiments were increased to account for variation among mice. Initial bone marrow transplants were replicated to test for variation in leukemia progression among different experiments. After this was ruled-out, bone marrow transplantation experiments were no longer replicated, but sample size was large and results were reproducible among animals. For testing the effect of MRK-560 on human PDX samples in mice, every experiment was performed only once with five mice per treatment intervention. However, three independent PDX samples were chosen to ensure reproducibility among different patient samples to test for a broader applicability of the approach. Once conditions for an experiment were optimized, all data were included in the absence of a specific technical or procedural reason that confounded the interpretation of a finding. For bioluminescence imaging, the value from one vehicle mouse on day 21 was excluded from the analysis, due for technical reasons due to an incorrect IP injection. Bioluminescence values for this mouse before and after day 21 are present in the analysis. For histological analysis for intestinal toxicity, investigators were blinded during goblet cell counting. During data collection and analysis investigators were blinded to group allocation.

Cell culture, expression plasmids and retrovirus production. HPB-ALL, DND41 and Jurkat cell lines were cultured in RPMI medium supplemented with 20% Fetal Bovine Serum (FBS). HEK293T cells were cultured in RPMI medium supplemented with 10% FBS. Mouse Embryonic Fibroblasts (MEFs) knockout for *Psen* and *Aph1* rescued with *PSEN1* and *APH1A* or *PSEN2* and *APH1A* expression were described previously *(12)*. MEFs were transduced with pMSCV-NOTCH1ΔE-RFP-puromycin viral vectors and after puromycin selection, RFP-positive cells were selected through FACS sorting and cultured in DMEM/F12 medium supplemented with 10% FBS. All other constructs used were cloned into the pMSCV-IRES-GFP vector. Viral vectors were produced in HEK293T cells using an EcoPack

packaging plasmid and Genejuice transfection reagent (Merck-Millipore) and virus was harvested 48 h post transfection. The stromal cell-free culture system used to generate mouse pro-T cells was described previously *(36, 61)* and is summarized in supplement.

Compounds. DAPT was a kind gift from Janssen Pharmaceutica and DBZ ((S)-2-(2-(3,5-Difluorophenyl)acetamido)-N-((S)-5-methyl-6-oxo-6,7-dihydro-5H-dibenzo[b,d]azepin-7-yl) propanamide) was purchased from Selleckchem. Dimethylsulphoxide (DMSO) was purchased from VWR and (2-Hydroxypropyl)-β-cyclodextrin, meglumine, corn-oil and tamoxifen were purchased from Sigma-Aldrich. MRK-560 (*N*-[4-(4-chlorophenyl)sulfonyl-4-(2,5-difluorophenyl)cyclohexyl]-1,1,1-trifluoro methanesulfonamide) was kindly provided by Janssen Pharmaceutica and synthesized as described in supplement *(62)*.

Gene expression profiling. Human thymocytes were extracted from thymus tissue from children undergoing cardiac surgery and were obtained and used according to the guidelines of the Medical Ethical Commission of the Ghent University Hospital, Belgium. Fluorescence-activated cell sorter (FACS)-mediated cell sorting was used to isolate the different thymocyte subsets, representing the different stages of normal T cell development, as described previously *(63, 64)*.

GEO accession codes for publicly available datasets. Data for PSEN1 and PSEN2 expression in human small intestine was obtained from the GTEx portal and dbGaP accession number phs000424.vN.pN. RNA-sequencing data from T-ALL cell lines and T-ALL patient samples was published previously *(31, 32)*. RNA-sequencing data on T-ALL cell lines is available in the EGA database with accession number EGAD00001000849. RNA-seq data for human T-ALL can be accessed at https://ocg.cancer.gov/programs/target/data-matrix.

Mice and animal procedures. All experiments were approved by the Ethical Committee on Animal Experimenting of the University of Leuven. The generation of the different strains is described in.

supplement. Bone marrow transplantation to generate the mouse model for ΔEGF-NOTCH1-L1601P-ΔP was performed as described *(65)*.

Patient-derived xenografts. Human leukemic bone marrow cells from NOTCH1 mutant T-ALL patients 389E, XC63, XC65 and XB47 (**Supplementary Table S2**) were injected into the tail vein of 6 to 12 week old female NOD.Cg-Prkdc^{scid} Il2rg^{tm1Wjl}/SzJ (NSG) mice. After successful engraftment, splenocytes were harvested and reinjected at a concentration of 1×10^6 cells into secondary recipient NSG mice to create secondary transplants. Human leukemic cells were identified in peripheral blood samples by anti-hCD45 (APC, eBioscience) staining by flow cytometry or by luciferase *in vivo* bioimaging using the IVIS Spectrum (Caliper Lifesciences). After the leukemic clone was detectable in the blood or by bioimaging, mice were segregated randomly into treatment groups and treated daily for 14 days with vehicle or MRK-560 (30 μmol/kg) dissolved in 20% hydroxypropyl-β-cyclodextrin (HPβCD) in 0.1 M meglumine by subcutaneous injection.

Statistical analyses. Graphs are presented as mean ± standard deviation and all analysis were performed using GraphPad Prism. Comparison between two groups was performed by the Student's unpaired two-tailed t test. One-way Anova was used to examine differences when comparing effects in three groups, i.e. comparing wild type, Psen1$^{f/f}$ and CD2CrePsen1$^{\Delta/\Delta}$ for leukemia progression, T cell development and in *ex vivo* T cell cultures. For measuring cell growth of T-ALL cells or leukemia progression in patient-derived xenograft models over time, differences were assessed by two-way Anova. Tukey post-hoc analysis was performed to correct for multiple comparisons. Survival in mouse experiments was represented with Kaplan-Meier survival curves and statistical significance was calculated using the log-rank test.

List of Supplementary Materials

Supplementary Methods

Fig. S1. Psen1 deletion does not affect T cell development.

Fig. S2. Psen1 deletion does not affect engraftment in bone marrow transplants.

Fig. S3. Tamoxifen does not affect leukemia progression

Fig. S4. MRK-560 shows selectivity for PSEN1 over PSEN2.

Fig. S5. Treatment of patient-derived xenograft samples with MRK-560

Fig. S6. Long term treatment with MRK-560 leads to significantly less gastrointestinal toxicity compared to DBZ

Table S1. Primers used for qPCR

Table S2. T-ALL patient-derived xenograft samples

References

1. N. Jurisch-Yaksi, R. Sannerud, W. Annaert, A fast growing spectrum of biological functions of γ-secretase in development and disease, *Biochim. Biophys. Acta* **1828**, 2815–27 (2013).

2. J. H. van Es, M. E. van Gijn, O. Riccio, M. van den Born, M. Vooijs, H. Begthel, M. Cozijnsen, S. Robine, D. J. Winton, F. Radtke, H. Clevers, Notch/γ-secretase inhibition turns proliferative cells in intestinal crypts and adenomas into goblet cells, *Nature* **435**, 959–963 (2005).

3. P. Doerfler, M. S. Shearman, R. M. Perlmutter, Presenilin-dependent gamma-secretase activity modulates thymocyte development, *Proc. Natl. Acad. Sci. U.S.A.* **98**, 9312–7 (2001).

4. G. T. Wong, D. Manfra, F. M. Poulet, Q. Zhang, H. Josien, T. Bara, L. Engstrom, M. Pinzon-Ortiz, J. S. Fine, H. J. Lee, L. Zhang, G. A. Higgins, E. M. Parker, Chronic treatment with the gamma-secretase inhibitor LY-411,575 inhibits beta-amyloid peptide production and alters lymphopoiesis and intestinal cell differentiation, *J. Biol. Chem.* **279**, 12876–82 (2004).

5. M. C. de Vera Mudry, F. Regenass-Lechner, L. Ozmen, B. Altmann, M. Festag, T. Singer, L. Müller, H. Jacobsen, A. Flohr, Morphologic and functional effects of gamma secretase inhibition on splenic marginal zone B cells, *Int J Alzheimers Dis* **2012**, 289412 (2012).

6. R. S. Doody, R. Raman, M. Farlow, T. Iwatsubo, B. Vellas, S. Joffe, K. Kieburtz, F. He, X. Sun, R. G. Thomas, P. S. Aisen, E. Siemers, G. Sethuraman, R. Mohs, A. D. C. S. S. Committee, S. S. Group, A phase 3 trial of semagacestat for treatment of Alzheimer's disease, *N. Engl. J. Med.* **369**, 341–50 (2013).

7. B. De Strooper, W. Annaert, P. Cupers, P. Saftig, K. Craessaerts, J. S. Mumm, E. H. Schroeter, V. Schrijvers, M. S. Wolfe, W. J. Ray, A. Goate, R. Kopan, A presenilin-1-dependent gamma-secretase-like protease mediates release of Notch intracellular domain, *Nature* **398**, 518–22 (1999).

8. W. T. Kimberly, M. J. LaVoie, B. L. Ostaszewski, W. Ye, M. S. Wolfe, D. J. Selkoe, Gamma-secretase is a membrane protein complex comprised of presenilin, nicastrin, Aph-1, and Pen-2, *Proc. Natl. Acad. Sci. U.S.A.* **100**, 6382–7 (2003).

9. B. De Strooper, Aph-1, Pen-2, and Nicastrin with Presenilin generate an active gamma-Secretase complex, *Neuron* **38**, 9–12 (2003).

10. S. S. Hébert, L. Serneels, T. Dejaegere, K. Horré, M. Dabrowski, V. Baert, W. Annaert, D. Hartmann, B. De Strooper, Coordinated and widespread expression of gamma-secretase in vivo: evidence for size and molecular heterogeneity, *Neurobiol Dis* **17**, 260–72 (2004).

11. R. Sannerud, C. Esselens, P. Ejsmont, R. Mattera, L. Rochin, A. K. Tharkeshwar, G. De Baets, V. De Wever, R. Habets, V. Baert, W. Vermeire, C. Michiels, A. J. Groot, R. Wouters, K. Dillen, K. Vints, P. Baatsen, S. Munck, R. Derua, E. Waelkens, G. S. Basi, M. Mercken, M. Vooijs, M. Bollen, J. Schymkowitz, F. Rousseau, J. S. Bonifacino, G. Van Niel, B. De Strooper, W. Annaert, Restricted Location of PSEN2/γ-Secretase Determines Substrate Specificity and Generates an Intracellular Aβ Pool, *Cell* **166**, 193–208 (2016).

12. H. Acx, L. Chávez-Gutiérrez, L. Serneels, S. Lismont, M. Benurwar, N. Elad, B. De Strooper, Signature amyloid β profiles are produced by different γ-secretase complexes, *Journal of Biological Chemistry* **289**, 4346–55 (2014).

13. H. Acx, L. Serneels, E. Radaelli, S. Muyldermans, C. Vincke, E. Pepermans, U. Müller, L. Chávez-Gutiérrez, B. De Strooper, Inactivation of γ-secretases leads to accumulation of substrates and non-Alzheimer neurodegeneration, *EMBO Mol Med* **9**, 1088–1099 (2017).

14. Wong, P. C., H. Zheng, H. Chen, M. W. Becher, D. J. Sirinathsinghji, M. E. Trumbauer, H. Y. Chen, D. L. Price, L. H. Van der Ploeg, S. S. Sisodia, Presenilin 1 is required for Notch1 and DII1 expression in the paraxial mesoderm, *Nature* **387**, 288–92 (1997).

15. J. Shen, R. T. Bronson, D. F. Chen, W. Xia, D. J. Selkoe, S. Tonegawa, Skeletal and CNS defects in Presenilin-1-deficient mice, *Cell* **89**, 629–39 (1997).

16. L. Serneels, T. Dejaegere, K. Craessaerts, K. Horré, E. Jorissen, T. Tousseyn, S. Hébert, M. Coolen, G. Martens, A. Zwijsen, W. Annaert, D. Hartmann, B. De Strooper, Differential contribution of the three Aph1 genes to gamma-secretase activity in vivo, *Proc. Natl. Acad. Sci. U.S.A.* **102**, 1719–24 (2005).

17. T. Dejaegere, L. Serneels, M. K. Schäfer, J. Van Biervliet, K. Horré, C. Depboylu, D. Alvarez-Fischer, A. Herreman, M. Willem, C. Haass, G. U. Höglinger, R. D'Hooge, B. De Strooper, Deficiency of Aph1B/C-gamma-secretase disturbs Nrg1 cleavage and sensorimotor gating that can be reversed with antipsychotic treatment, *Proc. Natl. Acad. Sci. U.S.A.* **105**, 9775–80 (2008).

18. L. Serneels, J. Van Biervliet, K. Craessaerts, T. Dejaegere, K. Horré, T. Van Houtvin, H. Esselmann, S. Paul, M. K. Schäfer, O. Berezovska, B. T. Hyman, B. Sprangers, R. Sciot, L. Moons, M. Jucker, Z. Yang, May, P. C., E. Karran, J. Wiltfang, R. D'Hooge, B. De Strooper, gamma-Secretase heterogeneity in the Aph1 subunit: relevance for Alzheimer's disease, *Science* **324**, 639–42 (2009).

19. A. Herreman, D. Hartmann, W. Annaert, P. Saftig, K. Craessaerts, L. Serneels, L. Umans, V. Schrijvers, F. Checler, H. Vanderstichele, V. Baekelandt, R. Dressel, P. Cupers, D. Huylebroeck, A. Zwijsen, F. Van Leuven, B. De Strooper, Presenilin 2 deficiency causes a mild pulmonary phenotype and no changes in amyloid precursor protein processing but enhances the embryonic lethal phenotype of presenilin 1 deficiency, *Proc. Natl. Acad. Sci. U.S.A.* **96**, 11872–7 (1999).

20. T. Palomero, A. Ferrando, Oncogenic NOTCH1 control of MYC and PI3K: challenges and opportunities for anti-NOTCH1 therapy in T-cell acute lymphoblastic leukemias and lymphomas, *Clin. Cancer Res.* **14**, 5314–7 (2008).

21. T. Girardi, C. Vicente, J. Cools, K. De Keersmaecker, The genetics and molecular biology of T-ALL, *Blood* **129**, 1113–1123 (2017).

22. P. Van Vlierberghe, A. Ferrando, The molecular basis of T cell acute lymphoblastic leukemia, *J. Clin. Invest.* **122**, 3398–406 (2012).

23. W. S. Pear, J. C. Aster, M. L. Scott, R. P. Hasserjian, B. Soffer, J. Sklar, D. Baltimore, Exclusive development of T cell neoplasms in mice transplanted with bone marrow expressing activated Notch alleles, *J. Exp. Med.* **183**, 2283–91 (1996).

24. A. P. Weng, A. A. Ferrando, W. Lee, J. P. Morris, L. B. Silverman, C. Sanchez-Irizarry, S. C. Blacklow, A. T. Look, J. C. Aster, Activating mutations of NOTCH1 in human T cell acute lymphoblastic leukemia, *Science* **306**, 269–71 (2004).

25. M. R. Mansour, D. C. Linch, L. Foroni, A. H. Goldstone, R. E. Gale, High incidence of Notch-1 mutations in adult patients with T-cell acute lymphoblastic leukemia, *Leukemia* **20**, 537–9 (2006).

26. F. Radtke, A. Wilson, G. Stark, M. Bauer, J. van Meerwijk, H. R. MacDonald, M. Aguet, Deficient T cell fate specification in mice with an induced inactivation of Notch1, *Immunity* **10**, 547–58 (1999).

27. A. P. Weng, Y. Nam, M. S. Wolfe, W. S. Pear, J. D. Griffin, S. C. Blacklow, J. C. Aster, Growth suppression of pre-T acute lymphoblastic leukemia cells by inhibition of notch signaling, *Molecular and Cellular Biology* **23**, 655–64 (2003).

28. T. Palomero, M. L. Sulis, M. Cortina, P. J. Real, K. Barnes, M. Ciofani, E. Caparros, J. Buteau, K. Brown, S. L. Perkins, G. Bhagat, A. M. Agarwal, G. Basso, M. Castillo, S. Nagase, C. Cordon-Cardo, R. Parsons, J. C. Zúñiga-Pflücker, M. Dominguez, A. A. Ferrando, Mutational loss of PTEN induces resistance to NOTCH1 inhibition in T-cell leukemia, *Nat. Med.* **13**, 1203–10 (2007).

29. P. J. Real, V. Tosello, T. Palomero, M. Castillo, E. Hernando, E. de Stanchina, M. L. Sulis, K. Barnes, C. Sawai, I. Homminga, J. Meijerink, I. Aifantis, G. Basso, C. Cordon-Cardo, W. Ai, A. Ferrando, Gamma-secretase inhibitors reverse glucocorticoid resistance in T cell acute lymphoblastic leukemia, *Nat. Med.* **15**, 50–8 (2009).

30. P. Ranganathan, K. L. Weaver, A. J. Capobianco, Notch signalling in solid tumours: a little bit of everything but not all the time, *Nat. Rev. Cancer* **11**, 338–51 (2011).

31. Y. Liu, J. Easton, Y. Shao, J. Maciaszek, Z. Wang, M. R. Wilkinson, K. McCastlain, M. Edmonson, S. B. Pounds, L. Shi, X. Zhou, X. Ma, E. Sioson, Y. Li, M. Rusch, P. Gupta, D. Pei, C. Cheng, M. A. Smith, J. G. Auvil, D. S. Gerhard, M. V. Relling, N. J. Winick, A. J. Carroll, N. A. Heerema, E. Raetz, M. Devidas, C. L. Willman, R. C. Harvey, W. L. Carroll, K. P. Dunsmore, S. S. Winter, B. L. Wood, B. P. Sorrentino, J. R. Downing, M. L. Loh, S. P. Hunger, J. Zhang, C. G. Mullighan, The genomic landscape of pediatric and young adult T-lineage acute lymphoblastic leukemia, *Nat. Genet.* **49**, 1211–1218 (2017).

32. Z. K. Atak, V. Gianfelici, G. Hulselmans, K. De Keersmaecker, A. G. Devasia, E. Geerdens, N. Mentens, S. Chiaretti, K. Durinck, A. Uyttebroeck, P. Vandenberghe, I. Wlodarska, J. Cloos, R. Foà, F. Speleman, J. Cools, S. Aerts, Comprehensive analysis of transcriptome variation uncovers known and novel driver events in T-cell acute lymphoblastic leukemia, *PLoS Genet.* **9**, e1003997 (2013).

33. E. Waegemans, I. Van de Walle, J. De Medts, M. De Smedt, T. Kerre, B. Vandekerckhove, G. Leclercq, T. Wang, J. Plum, T. Taghon, Notch3 activation is sufficient but not required for inducing human T-lineage specification, *J. Immunol.* **193**, 5997–6004 (2014).

34. H. Yu, C. A. Saura, S. Y. Choi, L. D. Sun, X. Yang, M. Handler, T. Kawarabayashi, L. Younkin, B. Fedeles, M. A. Wilson, S. Younkin, E. R. Kandel, A. Kirkwood, J. Shen, APP processing and synaptic plasticity in presenilin-1 conditional knockout mice, *Neuron* **31**, 713–726 (2001).

35. J. de Boer, A. Williams, G. Skavdis, N. Harker, M. Coles, M. Tolaini, T. Norton, K. Williams, K. Roderick, A. J. Potocnik, D. Kioussis, Transgenic mice with hematopoietic and lymphoid specific expression of Cre, *Eur. J. Immunol.* **33**, 314–25 (2003).

36. S. Bornschein, S. Demeyer, R. Stirparo, O. Gielen, C. Vicente, E. Geerdens, B. Ghesquière, S. Aerts, J. Cools, C. E. de Bock, Defining the molecular basis of oncogenic cooperation between TAL1 expression and Pten deletion in T-ALL using a novel pro-T-cell model system, *Leukemia* (2017), doi:10.1038/leu.2017.328.

37. T. Borgegård, S. Gustavsson, C. Nilsson, S. Parpal, R. Klintenberg, A. L. Berg, S. Rosqvist, L. Serneels, S. Svensson, F. Olsson, S. Jin, H. Yan, J. Wanngren, A. Jureus, A. Ridderstad-Wollberg, P. Wollberg, K. Stockling, H. Karlström, A. Malmberg, J. Lund, P. I. Arvidsson, B. De Strooper, U. Lendahl, J. Lundkvist, Alzheimer's disease: presenilin 2-sparing γ-secretase inhibition is a tolerable Aβ peptide-lowering strategy, *J. Neurosci.* **32**, 17297–305 (2012).

38. Z. Kalender Atak, K. De Keersmaecker, V. Gianfelici, E. Geerdens, R. Vandepoel, D. Pauwels, M. Porcu, I. Lahortiga, V. Brys, W. G. Dirks, H. Quentmeier, J. Cloos, H. Cuppens, A. Uyttebroeck, P. Vandenberghe, J. Cools, S. Aerts, High accuracy mutation detection in leukemia on a selected panel of cancer genes, *PLoS ONE* **7**, e38463 (2012).

39. K. De Keersmaecker, I. Lahortiga, N. Mentens, C. Folens, L. Van Neste, S. Bekaert, P. Vandenberghe, M. D. Odero, P. Marynen, J. Cools, In vitro validation of gamma-secretase inhibitors alone or in combination with other anti-cancer drugs for the treatment of T-cell acute lymphoblastic leukemia, *Haematologica* **93**, 533–42 (2008).

40. D. Herranz, A. Ambesi-Impiombato, J. Sudderth, M. Sanchez-Martin, L. Belver, V. Tosello, L. Xu, A. A. Wendorff, M. Castillo, J. E. Haydu, J. Márquez, J. M. Matés, A. L. Kung, S. Rayport, C. Cordon-Cardo, R. J. DeBerardinis, A. A. Ferrando, Metabolic reprogramming induces resistance to anti-NOTCH1 therapies in T cell acute lymphoblastic leukemia, *Nat. Med.* **21**, 1182–1189 (2015).

41. A. W. Tolcher, W. A. Messersmith, S. M. Mikulski, K. P. Papadopoulos, E. L. Kwak, D. G. Gibbon, A. Patnaik, G. S. Falchook, A. Dasari, G. I. Shapiro, J. F. Boylan, Z. X. Xu, K. Wang, A. Koehler, J. Song, S. A. Middleton, J. Deutsch, M. Demario, R. Kurzrock, J. J. Wheler, Phase I study of RO4929097, a gamma secretase inhibitor of Notch signaling, in patients with refractory metastatic or locally advanced solid tumors, *J. Clin. Oncol.* **30**, 2348–53 (2012).

42. M. Aricò, M. G. Valsecchi, B. Camitta, M. Schrappe, J. Chessells, A. Baruchel, P. Gaynon, L. Silverman, G. Janka-Schaub, W. Kamps, C.-H. Pui, G. Masera, Outcome of treatment in children with Philadelphia chromosome-positive acute lymphoblastic leukemia, *N. Engl. J. Med.* **342**, 998–1006 (2000).

43. J. M. Ribera, J. J. Ortega, A. Oriol, P. Bastida, C. Calvo, J. M. Pérez-Hurtado, M. E. González-Valentín, V. Martín-Reina, A. Molinés, F. Ortega-Rivas, M. J. Moreno, C. Rivas, I. Egurbide, I. Heras, C. Poderós, E. Martínez-Revuelta, J. M. Guinea, E. del Potro, G. Deben, Comparison of intensive chemotherapy, allogeneic, or autologous stem-cell transplantation as postremission treatment for children with very high risk acute lymphoblastic leukemia: PETHEMA ALL-93 Trial, *J. Clin. Oncol.* **25**, 16–24 (2007).

44. K. Cullion, K. M. Draheim, N. Hermance, J. Tammam, V. M. Sharma, C. Ware, G. Nikov, V. Krishnamoorthy, P. K. Majumder, M. A. Kelliher, Targeting the Notch1 and mTOR pathways in a mouse T-ALL model, *Blood* **113**, 6172–81 (2009).

45. H. Xiong, A. Maraver, J.-A. Latkowski, T. Henderson, K. Schlessinger, Y. Ding, J. Shen, C. E. Tadokoro, J. J. Lafaille, Characterization of two distinct lymphoproliferative diseases caused by ectopic expression of the Notch ligand DLL4 on T cells, *PLoS ONE* **8**, e84841 (2013).

46. B. Gerby, C. S. Tremblay, M. Tremblay, S. Rojas-Sutterlin, S. Herblot, J. Hébert, G. Sauvageau, S. Lemieux, E. Lécuyer, D. F. Veiga, T. Hoang, SCL, LMO1 and Notch1 reprogram thymocytes into self-renewing cells, *PLoS Genet.* **10**, e1004768 (2014).

47. S. Goossens, P. Van Vlierberghe, Controlling pre-leukemic thymocyte self-renewal, *PLoS Genet.* **10**, e1004881 (2014).

48. J. Tatarek, K. Cullion, T. Ashworth, R. Gerstein, J. C. Aster, M. A. Kelliher, Notch1 inhibition targets the leukemia-initiating cells in a Tal1/Lmo2 mouse model of T-ALL, *Blood* **118**, 1579–90 (2011).

49. F. Armstrong, P. Brunet de la Grange, B. Gerby, M. C. Rouyez, J. Calvo, M. Fontenay, N. Boissel, H. Dombret, A. Baruchel, J. Landman-Parker, P. H. Roméo, P. Ballerini, F. Pflumio, NOTCH is a key regulator of human T-cell acute leukemia initiating cell activity, *Blood* **113**, 1730–40 (2009).

50. J. D. Best, D. W. Smith, M. A. Reilly, R. O'Donnell, H. D. Lewis, S. Ellis, N. Wilkie, T. W. Rosahl, P. A. Laroque, C. Boussiquet-Leroux, I. Churcher, J. R. Atack, T. Harrison, M. S. Shearman, The novel gamma secretase inhibitor N-[cis-4-[(4-chlorophenyl)sulfonyl]-4-(2,5-difluorophenyl)cyclohexyl]-1,1,1-trifluoromethanesulfonamide (MRK-560) reduces amyloid plaque deposition without evidence of notch-related pathology in the Tg2576 mouse, *J Pharmacol Exp Ther* **320**, 552–8 (2007).

51. L. Jones, H. Carol, K. Evans, J. Richmond, P. J. Houghton, M. A. Smith, R. B. Lock, A review of new agents evaluated against pediatric acute lymphoblastic leukemia by the Pediatric Preclinical Testing Program, *Leukemia* **30**, 2133–2141 (2016).

52. X. Xia, S. Qian, S. Soriano, Y. Wu, A. M. Fletcher, X. J. Wang, E. H. Koo, X. Wu, H. Zheng, Loss of presenilin 1 is associated with enhanced beta-catenin signaling and skin tumorigenesis, *Proc. Natl. Acad. Sci. U.S.A.* **98**, 10863–8 (2001).

53. X. S. Puente, M. Pinyol, V. Quesada, L. Conde, G. R. Ordóñez, N. Villamor, G. Escaramis, P. Jares, S. Beà, M. González-Díaz, L. Bassaganyas, T. Baumann, M. Juan, M. López-Guerra, D. Colomer, J. M. Tubío, C. López, A. Navarro, C. Tornador, M. Aymerich, M. Rozman, J. M. Hernández, D. A. Puente, J. M. Freije, G. Velasco, A. Gutiérrez-Fernández, D. Costa, A. Carrió, S. Guijarro, A. Enjuanes, L. Hernández, J. Yagüe, P. Nicolás, C. M. Romeo-Casabona, H. Himmelbauer, E. Castillo, J. C. Dohm, S. de Sanjosé, M. A. Piris, E. de Alava, J. San Miguel, R. Royo, J. L. Gelpí, D. Torrents, M. Orozco, D. G. Pisano, A. Valencia, R. Guigó, M. Bayés, S. Heath, M. Gut, P. Klatt, J. Marshall, K. Raine, L. A. Stebbings, P. A. Futreal, M. R. Stratton, P. J. Campbell, I. Gut, A. López-Guillermo, X. Estivill, E. Montserrat, C. López-Otín, E. Campo, Whole-genome sequencing identifies recurrent mutations in chronic lymphocytic leukaemia, *Nature* **475**, 101–5 (2011).

54. I. Krop, T. Demuth, T. Guthrie, P. Y. Wen, W. P. Mason, P. Chinnaiyan, N. Butowski, M. D. Groves, S. Kesari, S. J. Freedman, S. Blackman, J. Watters, A. Loboda, A. Podtelezhnikov, J. Lunceford, C. Chen, M. Giannotti, J. Hing, R. Beckman, P. Lorusso, Phase I pharmacologic and pharmacodynamic study of the gamma secretase (Notch) inhibitor MK-0752 in adult patients with advanced solid tumors, *J. Clin. Oncol.* **30**, 2307–13 (2012).

55. A. F. Schott, M. D. Landis, G. Dontu, K. A. Griffith, R. M. Layman, I. Krop, L. A. Paskett, H. Wong, L. E. Dobrolecki, M. T. Lewis, A. M. Froehlich, J. Paranilam, D. F. Hayes, M. S. Wicha, J. C. Chang, Preclinical and clinical studies of gamma secretase inhibitors with docetaxel on human breast tumors, *Clin. Cancer Res.* **19**, 1512–24 (2013).

56. K. Mizutari, M. Fujioka, M. Hosoya, N. Bramhall, H. J. Okano, H. Okano, A. S. Edge, Notch inhibition induces cochlear hair cell regeneration and recovery of hearing after acoustic trauma, *Neuron* **77**, 58–69 (2013).

57. Y. Tona, K. Hamaguchi, M. Ishikawa, T. Miyoshi, N. Yamamoto, K. Yamahara, J. Ito, T. Nakagawa, Therapeutic potential of a gamma-secretase inhibitor for hearing restoration in a guinea pig model with noise-induced hearing loss, *BMC Neurosci* **15**, 66 (2014).

58. F. Zhu, T. Li, F. Qiu, J. Fan, Q. Zhou, X. Ding, J. Nie, X. Yu, Preventive effect of Notch signaling inhibition by a gamma-secretase inhibitor on peritoneal dialysis fluid-induced peritoneal fibrosis in rats, *Am J Pathol* **176**, 650–9 (2010).

59. T. Aoyama, K. Takeshita, R. Kikuchi, K. Yamamoto, X. W. Cheng, J. K. Liao, T. Murohara, gamma-Secretase inhibitor reduces diet-induced atherosclerosis in apolipoprotein E-deficient mice, *Biochem. Biophys. Res. Commun.* **383**, 216–21 (2009).

60. D. Fukuda, E. Aikawa, F. K. Swirski, T. I. Novobrantseva, V. Kotelianski, C. Z. Gorgun, A. Chudnovskiy, H. Yamazaki, K. Croce, R. Weissleder, J. C. Aster, G. S. Hotamisligil, H. Yagita, M. Aikawa, Notch ligand delta-like 4 blockade attenuates atherosclerosis and metabolic disorders, *Proc. Natl. Acad. Sci. U.S.A.* **109**, E1868–77 (2012).

61. N. Gehre, A. Nusser, L. von Muenchow, R. Tussiwand, C. Engdahl, G. Capoferri, N. Bosco, R. Ceredig, A. G. Rolink, A stromal cell free culture system generates mouse pro-T cells that can reconstitute T-cell compartments in vivo, *Eur. J. Immunol.* **45**, 932–42 (2015).

62. I. Churcher, D. Beher, J. D. Best, J. L. Castro, E. E. Clarke, A. Gentry, T. Harrison, L. Hitzel, E. Kay, S. Kerrad, H. D. Lewis, P. Morentin-Gutierrez, R. Mortishire-Smith, P. J. Oakley, M. Reilly, D. E. Shaw, M. S. Shearman, M. R. Teall, S. Williams, J. D. J. Wrigley, 4-substituted cyclohexyl sulfones as potent, orally active gamma-secretase inhibitors, *Bioorg. Med. Chem. Lett.* **16**, 280–284 (2006).

63. S. Peirs, F. Matthijssens, S. Goossens, I. Van de Walle, K. Ruggero, C. E. de Bock, S. Degryse, K. Canté-Barrett, D. Briot, E. Clappier, T. Lammens, B. De Moerloose, Y. Benoit, B. Poppe, J. P. Meijerink, J. Cools, J. Soulier, T. H. Rabbitts, T. Taghon, F. Speleman, P. Van Vlierberghe, ABT-199 mediated inhibition of BCL-2 as a novel therapeutic strategy in T-cell acute lymphoblastic leukemia, *Blood* **124**, 3738–47 (2014).

64. T. Taghon, E. Waegemans, I. Van de Walle, Notch signaling during human T cell development, *Curr. Top. Microbiol. Immunol.* **360**, 75–97 (2012).

65. C. E. de Bock, S. Demeyer, S. Degryse, D. Verbeke, B. Sweron, O. Gielen, R. Vandepoel, C. Vicente, M. Vanden Bempt, A. Dagklis, E. Geerdens, S. Bornschein, R. Gijsbers, J. Soulier, J. P. Meijerink, M. Heinäniemi, S. Teppo, M. Bouvy-Liivrand, O. Lohi, E. Radaelli, J. Cools, HOXA9 Cooperates with Activated JAK/STAT Signaling to Drive Leukemia Development, *Cancer Discov* **8**, 616–631 (2018).

66. W. G. Annaert, C. Esselens, V. Baert, C. Boeve, G. Snellings, P. Cupers, K. Craessaerts, B. De Strooper, Interaction with telencephalin and the amyloid precursor protein predicts a ring structure for presenilins, *Neuron* **32**, 579–89 (2001).

67. C. Esselens, V. Oorschot, V. Baert, T. Raemaekers, K. Spittaels, L. Serneels, H. Zheng, P. Saftig, B. De Strooper, J. Klumperman, W. Annaert, Presenilin 1 mediates the turnover of telencephalin in hippocampal neurons via an autophagic degradative pathway, *J. Cell Biol.* **166**, 1041–54 (2004).

68. P. Bankhead, M. B. Loughrey, J. A. Fernández, Y. Dombrowski, D. G. McArt, P. D. Dunne, S. McQuaid, R. T. Gray, L. J. Murray, H. G. Coleman, J. A. James, M. Salto-Tellez, P. W. Hamilton, QuPath: Open source software for digital pathology image analysis, *Sci Rep* **7**, 16878 (2017).

Acknowledgements

Synthesis of MRK-560 took place at Janssen Pharmaceutica Neuroscience Medicinal Chemistry by RN, as a visiting scientist. **Funding:** This work was supported by the Fonds voor Wetenschappelijk Onderzoek - Vlaanderen (FWO), the KU Leuven and VIB, a Methusalem grant from the KU Leuven/Flemish Government to BDS. BDS is supported by the Bax-Vanluffelen Chair for Alzheimer's Disease and "Opening the Future" of the Leuven Universiteit Fonds (LUF). JC is supported by an ERC-consolidator grant (617340) and "Kom op tegen Kanker" (stand up to cancer), the Flemish cancer society. RH is supported by a FWO fellowship (12I2317N). **Author contributions:** RAH, CEDB, JC and BDS conceived the study, designed and analyzed experiments and prepared the manuscript. RAH and CEDB performed most of the experiments with the help of DN, IL, DV, LS, JD and AL. SD performed analysis of RNA-seq data and TT performed analysis of Micro-Array data. RN performed MRK-560 synthesis. All authors reviewed the manuscript and agreed with the final submission. **Competing interests:** BDS and RN received a grant from Janssen Pharmaceutica for the development of γ-secretase inhibitors. The other authors declare no competing interest. **Data and materials availability:** The dataset analysed during the current study to determine PSEN1 and PSEN2 expression in developing human thymocytes is not publicly available yet but available on reasonable request. RNA-sequencing data on T-ALL cell lines is available in the EGA database with accession number EGAD00001000849. RNA-seq data for human T-ALL can be accessed at https://ocg.cancer.gov/programs/target/data-matrix. Data for Fig5b was obtained from the GTEx portal, dbGaP accession number phs000424.vN.pN.

Figure legends

Fig. 1. Psen1 deletion specifically reduces oncogenic mutant NOTCH1 signaling in T cells.

(**A**) Schematic representation of the four different γ-secretase complexes that exist in humans. All complexes contain Nicastrin (NCSTN), Presenilin-enhancer-2 (PEN-2) and either APH-1A or APH-1B and Presenilin-1 (PS-1) or Presenilin-2 (PS-2). (**B**) *PSEN1* (probe X203460_s_at) and *PSEN2* (probe X211373_s_at) expression in sorted subsets of human thymocytes. Average expression and standard deviation in samples obtained from two different donors are shown. (**C**) RNA-sequencing FPKM *PSEN1* and *PSEN2* levels in T-ALL cell lines (ALL-SIL, CCRF-CEM, DND41, HPB-ALL, HSB2, Jurkat, Karpas45, KE37, LOUCY, MOLT14, MOLT4, P12-Ichikawa, PEER, PF382, RPMI-8402, RM2, SUPT1, SUPT13 & T-ALL1) and T-ALL patient samples. (**D**) Representative flow-cytometry plots of thymocyte populations stained with antibodies against CD4 and CD8 or CD44 and CD25 in C57BL/6 wild type, $Psen1^{f/f}$ or $CD2CrePsen1^{\Delta/\Delta}$ mice. (**E, F**) Quantification of thymic T cell populations in relative numbers (wild type: n=5, $Psen1^{f/f}$: n=4, $CD2CrePsen1^{\Delta/\Delta}$: n=4). (**G**) Relative cell numbers of *ex vivo* cultures of mouse pro-T cells derived from C57BL/6 wild type, $Psen1^{f/f}$ or $CD2CrePsen1^{\Delta/\Delta}$ mice grown for 7 days (n=3 for all). (**H**) Relative cell numbers of *ex vivo* cultures of mouse pro-T cells derived from C57BL/6 wild type (n=2), $Psen1^{f/f}$ (n=3) or $CD2CrePsen1^{\Delta/\Delta}$ (n=3) mice transduced with MSCV-NOTCH1-L1601P-ΔP-IRES-GFP grown for 7 days without Dll4 Notch ligand. (**I**) Western blot analysis of C57BL/6 wild type (n=4), $Psen1^{f/f}$ (n=4) or $CD2CrePsen1^{\Delta/\Delta}$ (n=3) NOTCH1-L1601P-ΔP pro-T cells for NICD1, Psen1, Psen2, Nicastrin and β-actin cultured in the absence of Dll4 for 72 hours. Quantification of NICD1 levels are shown on the right. NICD, Notch IntraCellular Domain. All graphs show the mean values and error bars represent standard deviation. P-values for **C** were calculated using two-tailed Student's t-test. **** $P \leq 0.0001$. P-values in **E**, **F**, **G**, **H** and **I** were calculated using one-way ANOVA. * $P \leq 0.05$, *** $P \leq 0.001$ and **** $P \leq 0.0001$.

Fig. 2. Psen1 deletion impairs mutant NOTCH1-induced T-ALL development.

(**A**) Schematic of primary bone marrow transplant using hematopoietic stem and progenitor cells from C57BL/6 wild type, $Psen1^{f/f}$ or $CD2CrePsen1^{\Delta/\Delta}$ donor mice transduced with MSCV-ΔEGF-NOTCH1-

L1601P-ΔP-IRES-GFP transplanted into sublethally irradiated wild type C57BL/6 recipient mice. (**B**) Representative flow cytometry plots for the levels of GFP+ transduced lineage-negative cells prior to injection into recipient mice, (**C**) Representative flow cytometry plots for levels of circulating GFP^+ cells in peripheral blood from mice transplanted with wild type, $Psen1^{f/f}$ or $CD2CrePsen1^{\Delta/\Delta}$ progenitors expressing ΔEGF-NOTCH1-L1601P-ΔP 6 weeks after transplantation. Quantification of the GFP^+ population is shown on the right (n=9, 14 and 14 mice, respectively). (**D**) Representative flow cytometry plots of peripheral blood stained with antibodies to CD4 and CD8 from mice transplanted with wild type, $Psen1^{f/f}$ or $CD2CrePsen1^{\Delta/\Delta}$ progenitors expressing ΔEGF-NOTCH1-L1601P-ΔP 6 weeks after transplantation. Quantification of the $CD4^+CD8^+$ double-positive (DP) population is shown on the right (n=9, 14 and 14 mice, respectively). (**E**) Size and weight of spleens from mice transplanted with wild type, $Psen1^{f/f}$ or $CD2CrePsen1^{\Delta/\Delta}$ progenitors expressing ΔEGF-NOTCH1-L1601P-ΔP 9 weeks after transplantation (n=3). (**F**) Quantification of GFP^+ cells in spleens from mice transplanted with wild type, $Psen1^{f/f}$ or $CD2CrePsen1^{\Delta/\Delta}$ progenitors expressing ΔEGF-NOTCH1-L1601P-ΔP 9 weeks after transplantation (n=3). (**G**) Kaplan-Meier survival curves of mice transplanted with wild type, $Psen1^{f/f}$ or $CD2CrePsen1^{\Delta/\Delta}$ progenitors expressing ΔEGF-NOTCH1-L1601P-ΔP progenitors. All graphs show the mean values and error bars represent standard deviation. (**H**) Representative flow cytometry of end stage leukemia in the different cohorts of mice. P-values in **C**, **D, E** and **F** were calculated using one-way ANOVA. * $P \leq 0.05$, ** $P \leq 0.01$, *** $P \leq 0.001$ and **** $P \leq 0.0001$. P-value in **F** was calculated using the log-rank test. **** $P \leq 0.0001$.

Fig. 3. Genetic targeting of Psen1 impairs mutant NOTCH1 leukemia maintenance.

(**A**) Schematic of primary bone marrow transplant using hematopoietic stem and progenitor cells from $R26Cre\text{-}ER^{T2}Psen1^{f/f}$ donor mice transduced with MSCV-ΔEGF-NOTCH1-L1601P-ΔP-IRES-GFP before transplantation into sublethally irradiated wild type C57BL/6 recipient mice. Following confirmed engraftment (3 weeks post transplantation), primary transplant mice either were treated with 100 mg/kg/day tamoxifen by IP injection on 5 consecutive days to delete Psen1 specifically in transplanted donor cells or vehicle or used for secondary/tertiary transplants prior to treatment with 100 mg/kg/day tamoxifen by IP injection on 5 consecutive days to delete Psen1. (**B**) Levels of circulating

GFP$^+$ cells in peripheral blood from mice transplanted with R26Cre-ER^{T2}Psen1$^{f/f}$ progenitors expressing ΔEGF-NOTCH1-L1601P-ΔP following tamoxifen or vehicle treatment 5 weeks (n=13 and n=14 mice, respectively) and 9 weeks post-transplant (n=9 and n=11 mice, respectively). (**C**) Spleen weight and quantification of GFP$^+$ cells in spleens from mice transplanted with R26Cre-ER^{T2}Psen1$^{f/f}$ progenitors expressing ΔEGF-NOTCH1-L1601P-ΔP 5 weeks after transplant, treated either with vehicle only or tamoxifen (n=3 mice). (**D**) Kaplan-Meier survival curves of primary R26Cre-ER^{T2}Psen1$^{f/f}$ transplant mice expressing ΔEGF-NOTCH1-L1601P-ΔP treated either with vehicle or tamoxifen. (**E**) Kaplan-Meier survival curves of tertiary R26Cre-ER^{T2}Psen1$^{f/f}$ mice expressing ΔEGF-NOTCH1-L1601P-ΔP treated either with vehicle or tamoxifen. Gray boxes represent treatment period. All graphs show the mean values and error bars represent standard deviation. P-values in **B** and **C** were calculated using two-tailed Student's t-test. ** $P \leq 0.01$, *** $P \leq 0.001$ and **** $P \leq 0.0001$. The P-value in **D** was calculated using the log-rank test. **** $P \leq 0.0001$.

Fig. 4. Presenilin-1 selective inhibition impairs T-ALL cell proliferation.

(**A**) Western blot analysis for NICD1 levels in HPB-ALL, DND41 and Jurkat cells in response to MRK-560 and DAPT treatment. (**B**) Proliferation of NOTCH-dependent HPB-ALL and DND41 cells and NOTCH-independent Jurkat cells in response to MRK-560 (n=3). (**C**) Cell cycle analysis of HPB-ALL cells treated with increasing doses of MRK-560. (**D**) Quantification of the percentage of cells in G1 phase of HPB-ALL and DND-41 cells upon treatment with increasing doses of MRK-560. (**E**) Kaplan-Meier survival curves for mice with ΔEGF-NOTCH1-L1601P-ΔP-induced leukemia treated with vehicle or 30μmol/kg/day MRK-560 for 14 days. Gray boxes represent treatment period. Graphs show the mean values, error bars represent standard deviation. P-values in **B** were calculated using two-way Anova, P-values in **C** were calculated using the log-rank test, * $P \leq 0.05$, ** $P \leq 0.01$ and **** $P \leq 0.0001$.

Fig. 5. Pharmacological Psen1 inhibition attenuates leukemia in patient-derived xenografts. Progression of human-CD45$^+$ cells in peripheral blood from mice transplanted with patient sample (**A**) 389E, (**B**) XC63 and (**C**) XC65 treated with vehicle or 30μmol/kg/day MRK-560 for 14 days. (**D**)

Representative bioluminescence images depicting mice with leukemia burden closest to the mean for mice transplanted with patient sample XC65, treated with vehicle or MRK-560 for 14 days and quantification in the right panel. (**E**,**F**,**G**) Spleen weight and quantification of human-CD45^{+} cells in spleens from mice transplanted with patient sample (**E**) 389E, (**F**) XC63 and (**G**) XC65 after 14 days treatment with vehicle or MRK-560 (n=3 for 389E and n=4 for XC63 and XC65). (**H**,**I**,**J**) Kaplan-Meier survival curves of mice transplanted with patient sample (**H**) 389E, (**I**) XC63 and (**J**) XC65 treated with vehicle or MRK-560 for 14 days with XC65 showing survival curve when MRK-560 treatment was started once leukemia burden was shown to be high in blood (~50% hCD45+ cells) (**K**) qPCR analysis of DTX1, NOTCH3 and MYC expression levels in splenocytes from mice transplanted with patient sample XC63 or XC65 after 14 days vehicle or MRK-560 treatment (n=4). Graphs show the mean values, error bars represent standard deviation. Gray boxes represent treatment period. P-values in **A**, **B**, **C** and **D** were calculated using two-way Anova and two-tailed Student's t-test, P-values in **E**, **F**, **G** and **K** were calculated using two-tailed Student's t-test and P-values in **H**, **I** and **J** were calculated using the log-rank test, ** $P \leq 0.01$, *** $P \leq 0.001$ and **** $P \leq 0.0001$.

Fig. 6. Pharmacological selective Psen1 targeting does not cause gastrointestinal toxicity or T cell developmental defects.

(**A**) Representative images of Periodic Acid-Schiff staining of intestines from mice treated with vehicle, MRK-560 or the broad-spectrum γ-secretase inhibitor Dibenzazepine (DBZ) for 14 days to assess the number of secretory goblet cells. Scale bars represent 100 μm. Quantification of the number of goblet cells per cm villus is shown on the right (vehicle n=4, MRK-560 n=4 and DBZ n=3, respectively). (**B**) *PSEN1* and *PSEN2* gene expression levels in small intestine. Data for this analysis was obtained from the GTEx portal and dbGaP accession number phs000424.vN.pN. (**C**) Representative flow-cytometry plots of thymocyte populations stained with antibodies to CD4 and CD8 or CD44 and CD25 in C57BL/6 mice treated with vehicle, MRK-560 or Dibenzazepine (DBZ) for 14 days. (**D, E**) Quantification of intrathymic T cell populations in relative numbers (vehicle n=5, MRK-560 n=5 and DBZ n=3, respectively). All graphs show the mean values, error bars represent standard deviation. The P-values in

A, **D** and **E** were calculated using one-way ANOVA. * $P \leq 0.05$, ** $P \leq 0.01$, *** $P \leq 0.001$ and **** $P \leq 0.0001$.

Fig. 1

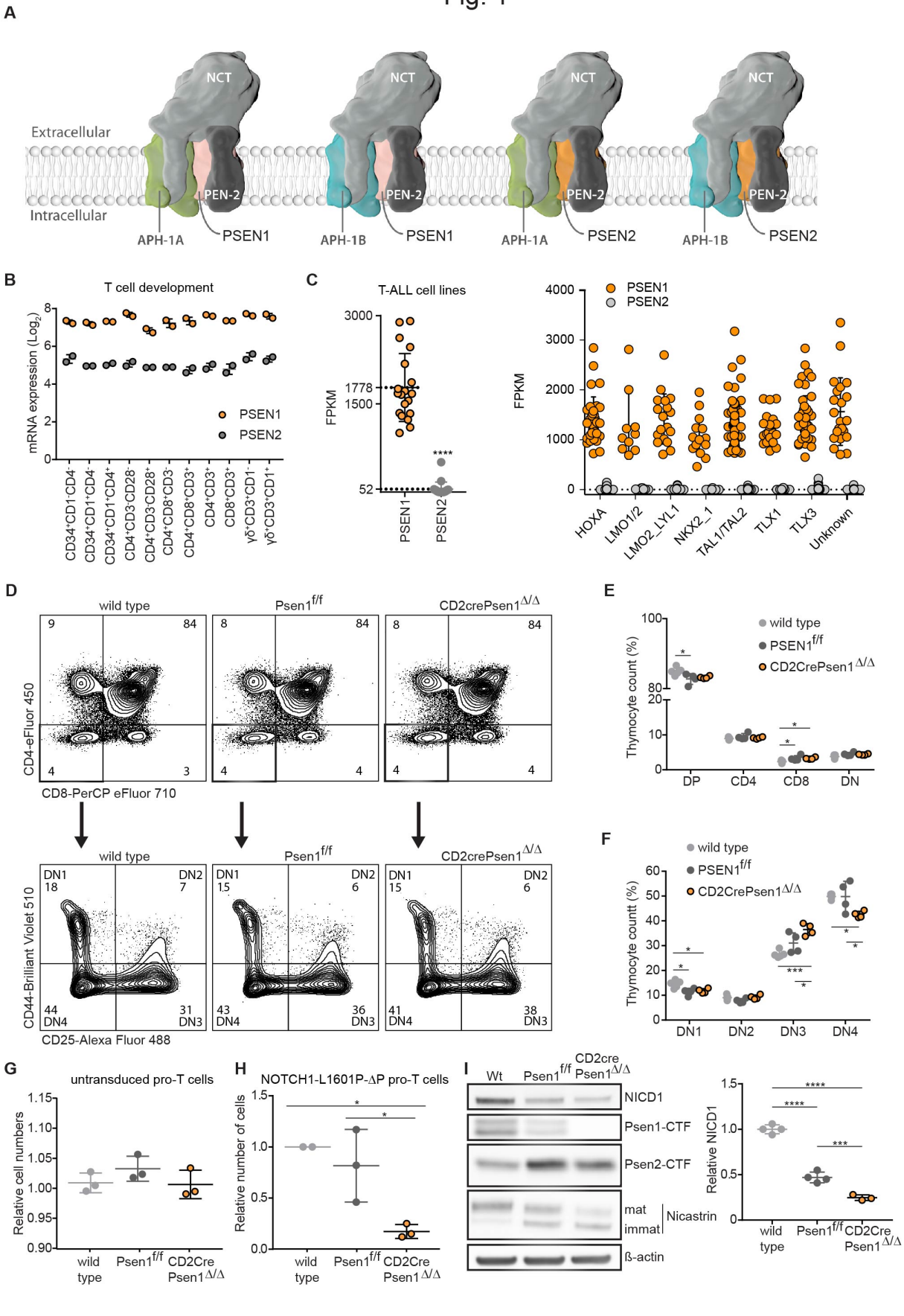
A
NCT
PEN-2
Extracellular
Intracellular
APH-1A
PSEN1
APH-1B
PSEN1
APH-1A
PSEN2
APH-1B
PSEN2
B
T cell development
mRNA expression (Log2)
PSEN1
PSEN2
CD34+CD1-CD4-
CD34+CD1+CD4-
CD34+CD1+CD4+
CD4+CD3-CD28-
CD4+CD3-CD28+
CD4+CD8+CD3-
CD4+CD8+CD3+
CD4+CD3+
CD8+CD3+
γδ+CD3+CD1-
γδ+CD3+CD1+
C
T-ALL cell lines
FPKM
3000
1778
1500
52
****
PSEN1
PSEN2
FPKM
4000
3000
2000
1000
0
PSEN1
PSEN2
HOXA
LMO1/2
LMO2_LYL1
NKX2_1
TAL1/TAL2
TLX1
TLX3
Unknown
D
wild type
Psen1f/f
CD2crePsen1Δ/Δ
CD4-eFluor 450
CD8-PerCP eFluor 710
9
84
4
3
8
84
4
4
8
84
4
4
CD44-Brilliant Violet 510
CD25-Alexa Fluor 488
DN1
18
DN2
7
44
DN4
31
DN3
DN1
15
DN2
6
43
DN4
36
DN3
DN1
15
DN2
6
41
DN4
38
DN3
E
wild type
PSEN1f/f
CD2CrePsen1Δ/Δ
Thymocyte count (%)
DP
CD4
CD8
DN
F
wild type
PSEN1f/f
CD2CrePsen1Δ/Δ
Thymocyte countt (%)
DN1
DN2
DN3
DN4
G
untransduced pro-T cells
Relative cell numbers
wild type
Psen1f/f
CD2Cre Psen1Δ/Δ
H
NOTCH1-L1601P-ΔP pro-T cells
Relative number of cells
wild type
Psen1f/f
CD2Cre Psen1Δ/Δ
I
Wt
Psen1f/f
CD2cre Psen1Δ/Δ
NICD1
Psen1-CTF
Psen2-CTF
mat
immat
Nicastrin
ß-actin
Relative NICD1
wild type
Psen1f/f
CD2Cre Psen1Δ/Δ

Fig. 2

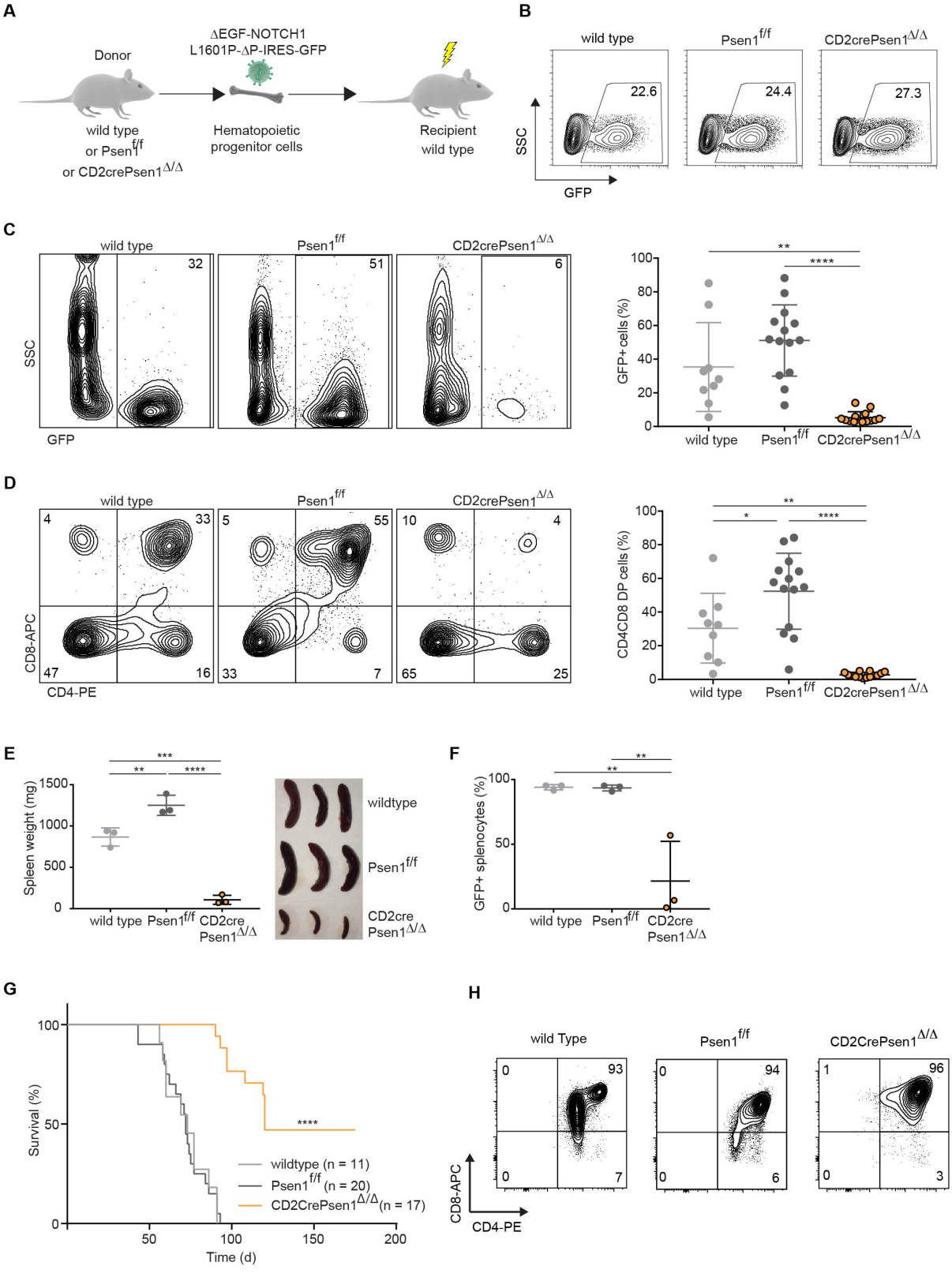
A
Donor
wild type
or Psen1f/f
or CD2crePsen1Δ/Δ
ΔEGF-NOTCH1
L1601P-ΔP-IRES-GFP
Hematopoietic
progenitor cells
Recipient
wild type
B
wild type
Psen1f/f
CD2crePsen1Δ/Δ
22.6
24.4
27.3
SSC
GFP
C
wild type
Psen1f/f
CD2crePsen1Δ/Δ
32
51
6
SSC
GFP
GFP+ cells (%)
D
4
33
47
16
5
55
33
7
10
4
65
25
CD8-APC
CD4-PE
CD4CD8 DP cells (%)
E
Spleen weight (mg)
wildtype
Psen1f/f
CD2cre
Psen1Δ/Δ
F
GFP+ splenocytes (%)
G
Survival (%)
Time (d)
wildtype (n = 11)
Psen1f/f (n = 20)
CD2CrePsen1Δ/Δ (n = 17)
H
wild Type
Psen1f/f
CD2CrePsen1Δ/Δ
0
93
0
7
0
94
0
6
1
96
0
3
CD8-APC
CD4-PE

Fig. 3

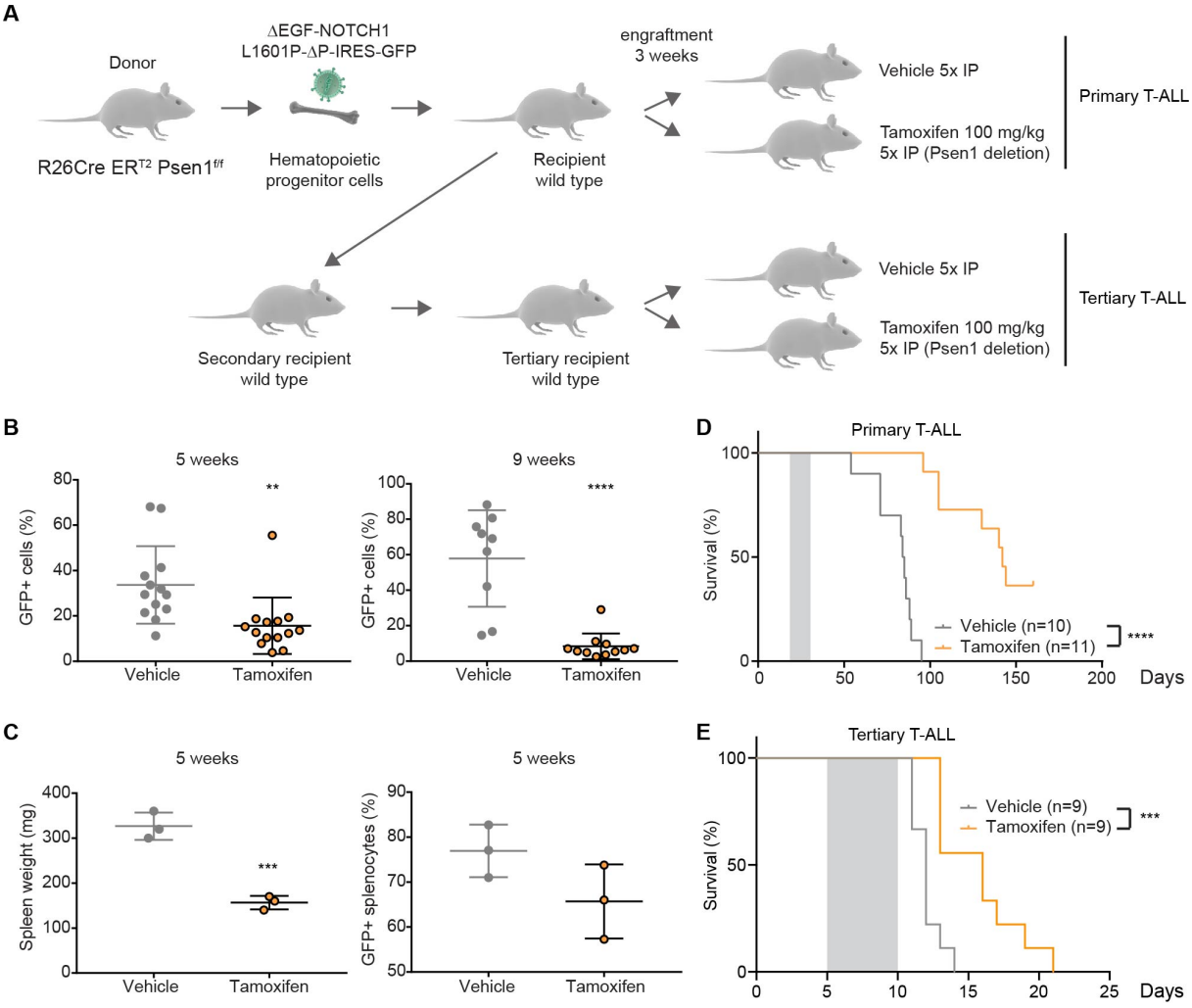
A
Donor
R26Cre ER^{T2} Psen1$^{f/f}$
ΔEGF-NOTCH1
L1601P-ΔP-IRES-GFP
Hematopoietic progenitor cells
Recipient wild type
engraftment 3 weeks
Vehicle 5x IP
Tamoxifen 100 mg/kg 5x IP (Psen1 deletion)
Primary T-ALL
Secondary recipient wild type
Tertiary recipient wild type
Vehicle 5x IP
Tamoxifen 100 mg/kg 5x IP (Psen1 deletion)
Tertiary T-ALL
B
5 weeks
GFP+ cells (%)
Vehicle
Tamoxifen
9 weeks
GFP+ cells (%)
Vehicle
Tamoxifen
C
5 weeks
Spleen weight (mg)
Vehicle
Tamoxifen
5 weeks
GFP+ splenocytes (%)
Vehicle
Tamoxifen
D
Primary T-ALL
Survival (%)
Vehicle (n=10)
Tamoxifen (n=11)
Days
E
Tertiary T-ALL
Survival (%)
Vehicle (n=9)
Tamoxifen (n=9)
Days

Fig. 4

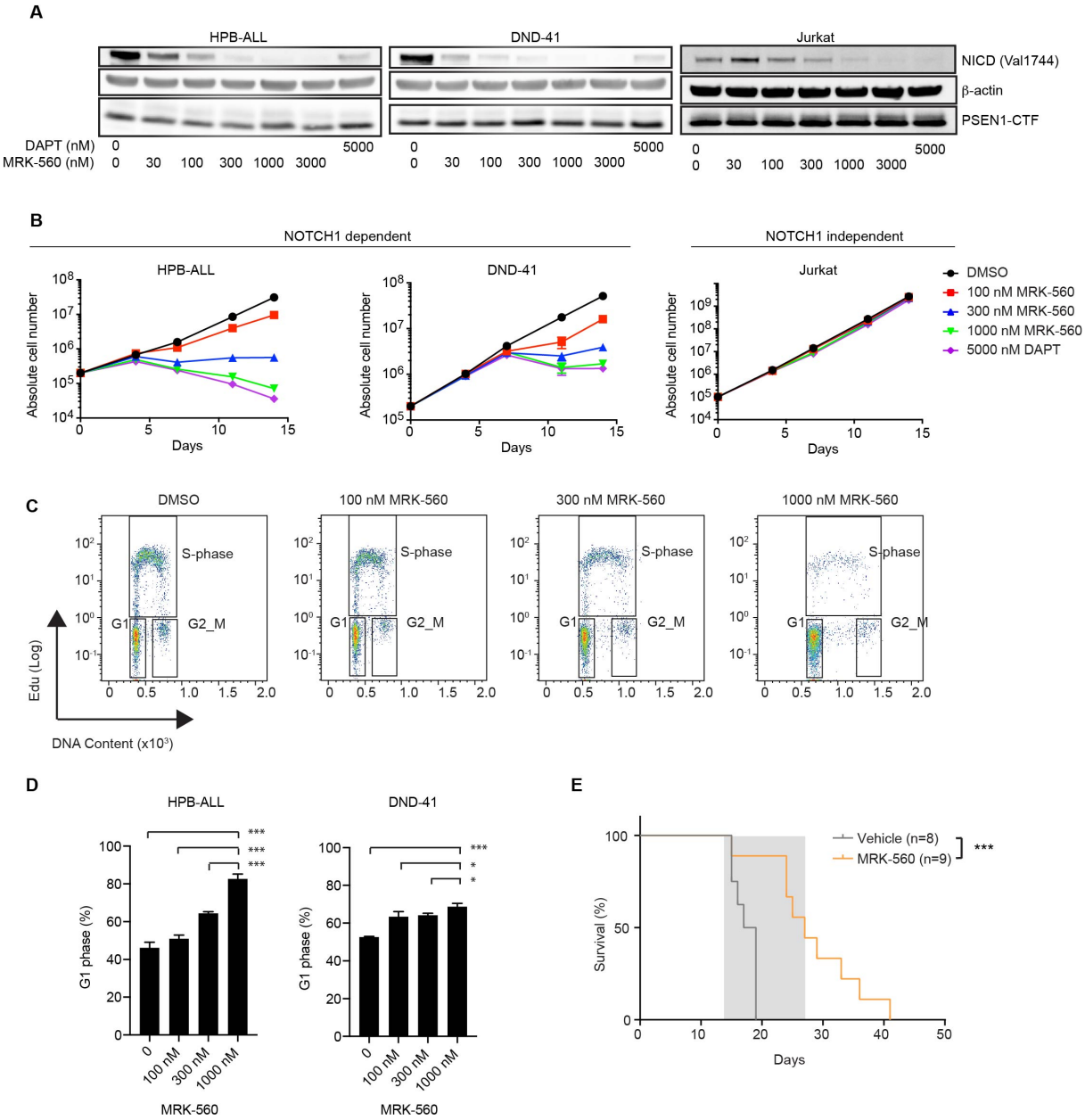
A
HPB-ALL
DND-41
Jurkat
NICD (Val1744)
β-actin
PSEN1-CTF
DAPT (nM)
MRK-560 (nM)
B
NOTCH1 dependent
NOTCH1 independent
Absolute cell number
Days
DMSO
100 nM MRK-560
300 nM MRK-560
1000 nM MRK-560
5000 nM DAPT
C
S-phase
G1
G2_M
Edu (Log)
DNA Content (x10³)
D
G1 phase (%)
MRK-560
E
Survival (%)
Vehicle (n=8)
MRK-560 (n=9)
***
Days

Fig. 5

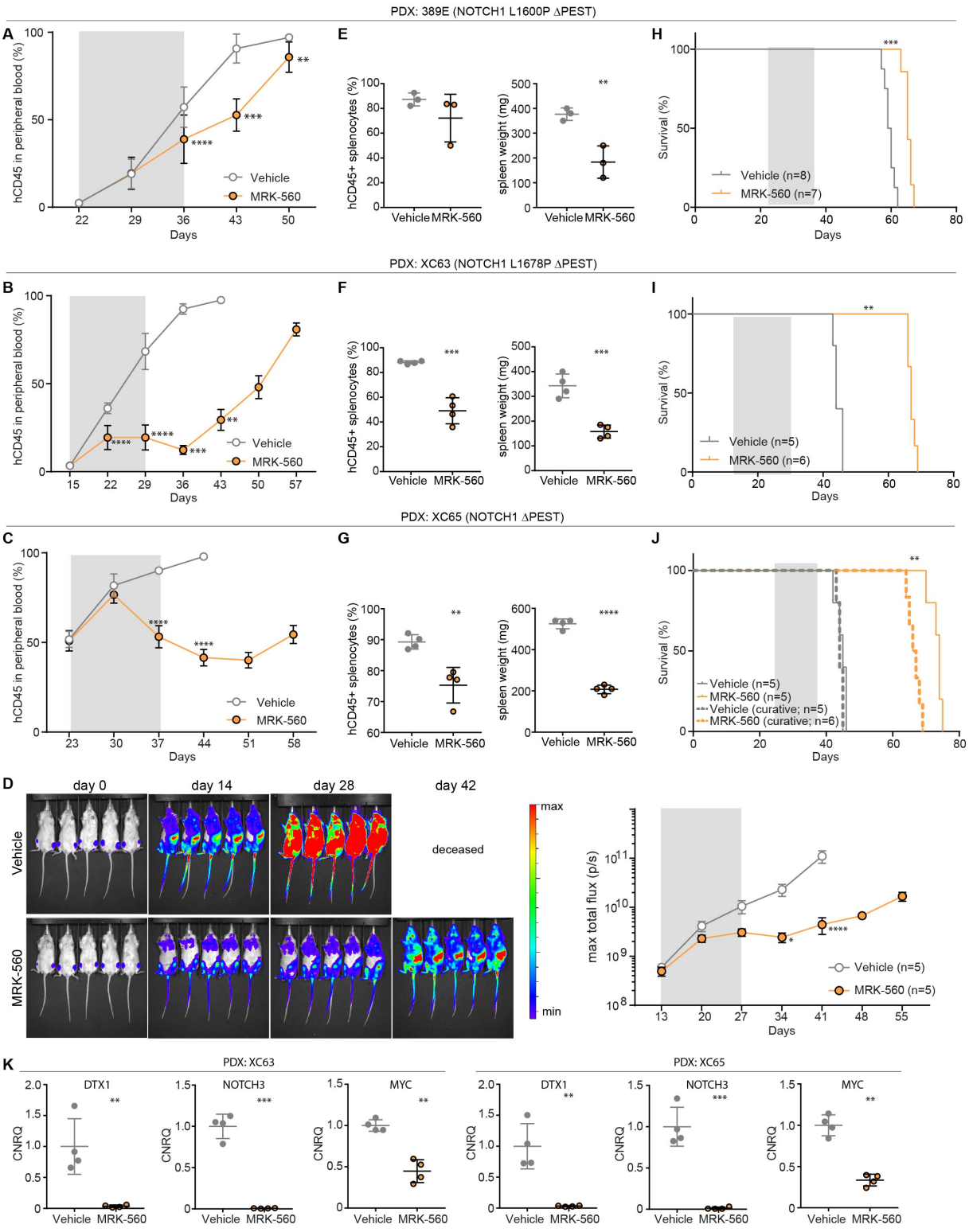
PDX: 389E (NOTCH1 L1600P ΔPEST)
A
hCD45 in peripheral blood (%)
Days
Vehicle
MRK-560
E
hCD45+ splenocytes (%)
spleen weight (mg)
Vehicle MRK-560
H
Survival (%)
Vehicle (n=8)
MRK-560 (n=7)
PDX: XC63 (NOTCH1 L1678P ΔPEST)
B
F
I
Vehicle (n=5)
MRK-560 (n=6)
PDX: XC65 (NOTCH1 ΔPEST)
C
G
J
Vehicle (n=5)
MRK-560 (n=5)
Vehicle (curative; n=5)
MRK-560 (curative; n=6)
D
day 0
day 14
day 28
day 42
deceased
max
min
max total flux (p/s)
Vehicle (n=5)
MRK-560 (n=5)
K
PDX: XC63
PDX: XC65
DTX1
NOTCH3
MYC
CNRQ

Fig. 6

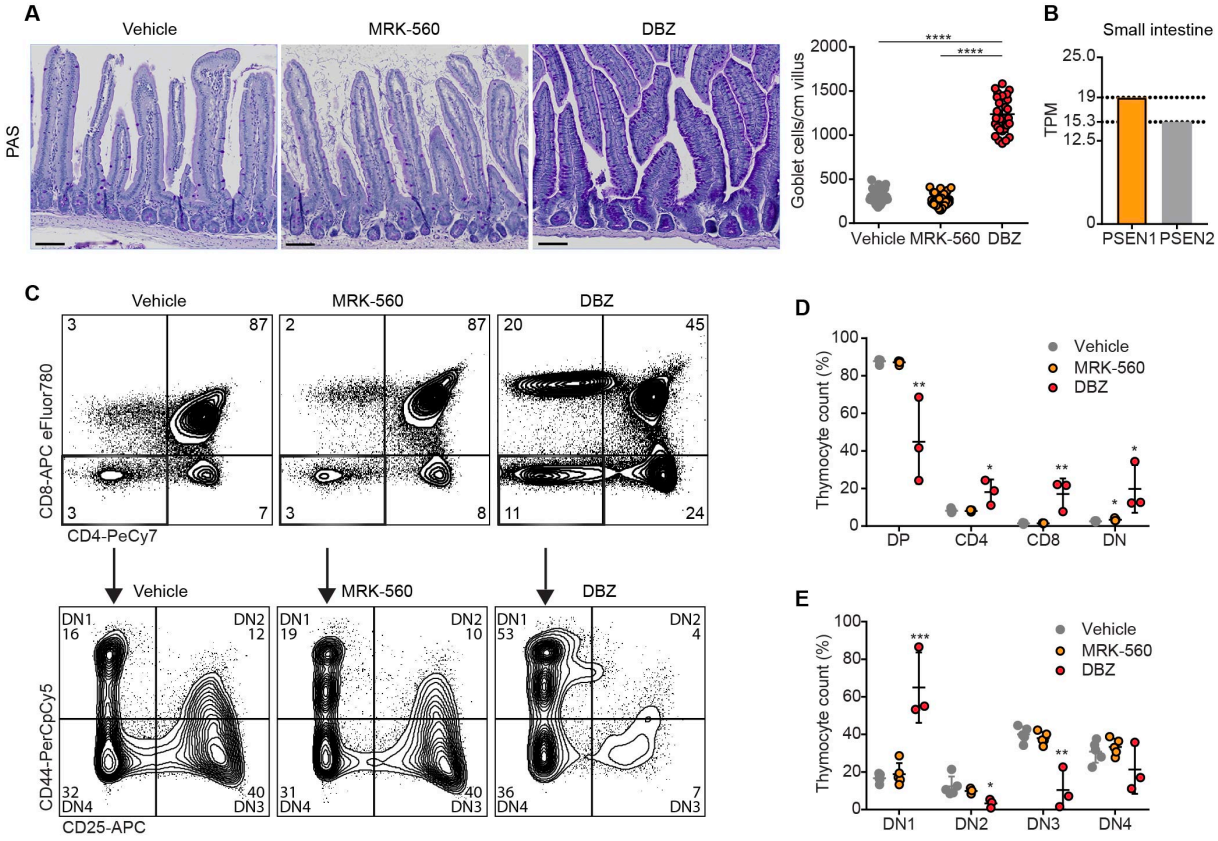
A
Vehicle
MRK-560
DBZ
PAS
Goblet cells/cm villus
2000
1500
1000
500
0
****
****
Vehicle MRK-560 DBZ
B
Small intestine
TPM
25.0
19
15.3
12.5
0
PSEN1 PSEN2
C
Vehicle
MRK-560
DBZ
CD8-APC eFluor780
CD4-PeCy7
3
87
3
7
2
87
3
8
20
45
11
24
CD44-PerCpCy5
CD25-APC
DN1
DN2
DN3
DN4
16
12
32
40
19
10
31
40
53
4
36
7
D
Thymocyte count (%)
Vehicle
MRK-560
DBZ
DP
CD4
CD8
DN
E
Thymocyte count (%)
Vehicle
MRK-560
DBZ
DN1
DN2
DN3
DN4

Supplementary Material

Safe targeting of T cell acute lymphoblastic leukemia by pathology specific NOTCH inhibition

Roger A. Habets, Charles E. de Bock, Lutgarde Serneels, Inge Lodewijkx, Delphine Verbeke, David Nittner, Rajeshwar Narlawar, Sofie Demeyer, James Dooley, Adrian Liston, Tom Taghon, Jan Cools and Bart de Strooper

Supplementary Methods

Chemistry. MRK-560 (N-[4-(4-chlorophenyl)sulfonyl-4-(2,5-difluorophenyl)cyclohexyl]-1,1,1-trifluoro methanesulfonamide) was kindly provided by Janssen Pharmaceutica and synthesized as follows. 4-(4-chlorophenyl)sulfonyl-4-(2,5-difluorophenyl)cyclohexanamine was synthesized using the literature procedure (61). Trifluoromethanesulfonic anhydride (0.214 mL, 1.269 mmol) was added to a stirred solution of 4-(4-chlorophenyl)sulfonyl-4-(2,5-difluorophenyl)cyclohexanamine (200 mg, 0.518 mmol) and triethyl amine (0.177 mL, 1.273 mmol) in anhydrous dichloromethane (10 mL) at 0 °C and the reaction mixture was stirred further for 90 min under inert atmosphere. Upon completion (TLC), reaction mixture was warmed to ambient temperature and concentrated in vacuo. The residue was then diluted with ethyl acetate (50 mL), washed with 2N NaOH, water, brine, dried over anhydrous magnesium sulfate, filtered and concentrated in vacuo. The crude compound was purified by flash column chromatography using 15% ethyl acetate in n-heptane as eluent to afford the desired compound as colourless solid (215 mg, 80%). 1H NMR (400 MHz, DMSO-d6): 1.49 (br t, J=13.8 Hz, 2 H), 1.82 (br d, J=14.2 Hz, 2 H), 2.33 - 2.46 (m, 2 H), 2.52 - 2.62 (m, 2 H), 3.61 - 3.67 (m, 1 H), 7.11 - 7.24 (m, 2 H), 7.29 - 7.34 (m, 1 H), 7.34 - 7.39 (m, 2 H), 7.61 - 7.65 (m, 2 H), 9.76 (br d, J=5.3 Hz, 1 H) δ ppm. 13C NMR (100 MHz, DMSO-d6): 23.94 (br d, J=5.1 Hz, 1 C), 27.61 (br s, 1 C), 49.14 (s, 1 C), 69.90 (d, J=4.4 Hz, 1 C), 117.89 - 118.41 (m, 1 C), 118.42 - 118.76 (m, 1 C), 118.97 (dd, J=26.0, 4.0 Hz, 1 C), 120.76 (dd, J=11.7, 7.3 Hz, 1 C), 129.09 (s, 1 C), 131.66 (s, 1 C), 133.23 (s, 1 C), 139.56 (s, 1 C), 156.66 - 157.52 (m, 1 C), 159.54 (dd, J=62.7, 1.8 Hz, 1 C) δ ppm. 19F NMR (377 MHz, DMSO-d6): 117.99 (s, 1 F), -113.25 (s, 1 F), -77.39 (s, 1 F) δ ppm. LCMS (ESI): 535.1 [M+NH4]+, 516.1 [M-H]- Purity: 99% (retention time: 2.20 min).

Antibodies for Western blotting. Rabbit polyclonal antibodies against Aph1a (B80.3), Aph1b (B78.2), Nct (9C3) and Pen-2 (B126) were described previously *(66, 67)*. Rabbit anti-Cleaved-Notch1-Val1744 (D3B8), anti-Psen1-CTF (D39D1) and anti-Psen2-CTF (D30G3) were purchased from Cell Signaling, Mouse anti-beta-actin (A5441) from Sigma and Rabbit anti-tRFP (AB234) was from Evrogen.

Secondary antibodies were conjugated with horseradish peroxidase and bands were visualized using a cooled charge-coupled device camera (ImageQuant LAS-4000; GE Healthcare).

Western blotting. MEFs, T-ALL cell lines or single cell preparation from mouse tissues were lysed in STE buffer (250 mM sucrose, 5 mM Tris pH7, 1 mM EGTA) + 1% TX-100 and incubated on ice for 30 min. The supernatant was collected after centrifugation at 19,000 *g* for 30 min at 4 °C. Equal amounts of protein were separated on NuPAGE NOVEX Bis-Tris gels (Life Technologies).

Presenilin selectivity assay. MEFs cells expressing the specified γ-secretase complexes were treated with the different compounds as indicated for 18 h in DMEM/F12 supplemented with 2% FBS.

***Ex vivo* T cell cultures.** Bone marrow cells were isolated from femur and tibia. Lineage-negative cells were enriched by negative selection using biotinylated antibodies directed against non-hematopoietic stem cells and non-progenitor cells (CD5, CD11b, CD19, CD45R/B220, Ly6G/C(Gr-1), TER119, 7-4) and streptavidin-coated magnetic particles (RapidSpheres™, STEMCELL Technologies). Enriched cells were cultured on Dll4-Fc coated plates in the presence of mIL7 (20 ng/mL) and mSCF (20 ng/mL). After differentiation into DN2 stage pro-T cells ($CD44^{+}CD25^{+}$), cells were transduced with MSCV-NOTCH1-L1601P-ΔP-IRES-GFP and GFP-positive cells were sorted through FACS sorting (S3 cell sorter Bio Rad). To assess processing and signaling from transduced mutant NOTCH proteins, cells were cultured in the absence of Dll4 during the course of experiments unless stated otherwise.

Human primary leukemia samples. Clinical leukemia samples were obtained with informed consent at local institutions and all experiments were conducted on protocols approved by the Ethical Committee of the University of Leuven.

Mice and animal procedures. Psen1 conditional knockout mice (Psen1tm2.1Bdes) were generated by homologous recombination in E14 ES cell line by introducing two loxP sites flanking exon 1. The first loxP site was introduced in intron 1 and the second together with a Frt flanked Hygromycin B selection marker cassette in intron 2. In addition, a double tag encoding Calmodulin Binding Protein (CBP) and 3xFLAG was inserted immediately following the ATG start codon. F1 offsprings were crossed with Gt(ROSA)26Sortm1(FLP1)Dym strain and deletion of the selection cassette was confirmed by Southern Blotting and PCR analysis. To generate mice carrying a Psen1 deletion in all committed B and T cell progenitors, we crossed these mice harboring the conditional Psen1 targeted allele with a specific Cre deleter line B6.Cg-Tg(CD2-icre)4Kio/J (The Jackson Laboratory, #008520), generating $CD2CrePsen1^{\Delta/\Delta}$. To generate conditional inducible Psen1 knockout mice, we bred animals harboring the conditional Psen1 allele with B6.129-Gt(ROSA)26Sortm1(cre/ERT2)Tyj/J mice, which express a tamoxifen-inducible form of the Cre recombinase, generating $Rosa26Cre\text{-}ER^{t2}Psen1^{f/f}$ mice. All

colonies were kept on an inbred C57Bl/6J background, which were also used as wild type control animals and recipient animals for primary and secondary transplants. NOD.Cg-Prkdscid Il2rgtm1Wjl H2-Ab1tm1Gru Tg(HLA-DRB1)31Dmz/Szj (NSG) mice used for patient-derived xenograft experiments were purchased from Harlan Laboratories. During experiments mice were housed in individually ventilated cages enriched with wood-wool and shavings as bedding, given access to water and food *ad libitum and monitored daily.*

Murine bone marrow transplantation. Six to 12 week old male mice were sacrificed and bone marrow cells were harvested from femur and tibia. Lineage-negative cells were enriched by negative selection using biotinylated antibodies directed against non-hematopoietic stem cells and non-progenitor cells (CD5, CD11b, CD19, CD45R/B220, Ly6G/C(Gr-1), TER119, 7-4) and streptavidin-coated magnetic particles (RapidSpheres™, STEMCELL Technologies) and cultured overnight in RPMI with 20% FCS with IL3 (10 ng/mL, Peprotech), IL6 (10 ng/mL, Peprotech), SCF (50 ng/mL, Peprotech), and penicillin-streptomycin. The following day, $1x10^6$ cells were transduced by spinoculation (90 min at 2500 rpm) with viral supernatant (ΔEGF-NOTCH1-L1601P-ΔP) and 8 µg/mL polybrene. The following day, the cells were washed in PBS and injected (1×10^6 cells/0.3 mL) into the lateral tail vein of sublethally irradiated (5 Gy) syngeneic 8 to 12 week old female C57BL/6 recipient mice. For secondary transplants, leukemic T cells were obtained from splenic tissue derived from mice transplanted with ΔEGF-NOTCH1-L1601P-ΔP wild type cells. Following isolation, 1,000,000 cells were transplanted intravenously into sublethally irradiated (2.5 Gy) 8 to 10 week old wild type (C57BL/6) female recipient mice. To delete the *Psen1* gene in NOTCH1-induced mouse leukemia, animals were treated with 100 mg/kg tamoxifen by IP injection for 5 consecutive days.

In vivo imaging. For *in vivo* bioimaging, cells from NOTCH1 mutant T-ALL sample XC63 were injected into the tail vein of 6 to 12 week old NSG mice and human leukemic cell expansion was monitored through hCD45 staining on peripheral blood samples. After successful engraftment and leukemic disease development, mice were sacrificed and single cells were isolated from the spleen, containing >90% $hCD45^+$ cells. Splenocytes were transduced overnight with lentivirus pCH-SFFV-eGFP-P2A-fLuc and GFP-positive cells were sorted using a S3 Sorter (Bio-Rad) before being transplanted back into NSG mice via tail vein injection. Upon confirmation that leukemic cells were >95% GFP-positive, leukemic cells were isolated from spleen and re-transplanted into a larger cohort of NSG mice for treatment studies. For *in vivo* bioluminescence imaging, anesthesia was induced in an induction chamber with 2% isoflurane in 100% oxygen at a flow rate of 2 L/min and maintained in the IVIS with a 1.5% mixture at 0.5 L/min. Before each imaging session, the mice were injected subcutaneous with 126 mg/kg d-luciferin (Promega, Leiden, the Netherlands) dissolved in PBS (15 mg/mL). Next, they were positioned in the IVIS and consecutive 2 min frames were acquired until the maximum signal was reached. Data are reported as the total flux per second from the whole mouse.

Toxicity studies, immunohistochemistry, immunofluorescence and flow cytometry. Healthy 12 week old C57BL/6 mice were treated for 14 days with vehicle (20% hydroxypropyl-β-cyclodextrin (HPβCD) in 0.1 M meglumine) or 30 μmol/kg MRK-560 by subcutaneous injection or 10 μmol/kg DBZ or vehicle (0.5% Methylcellulose, 0.1% Tween80) by IP injection. For the intermittent 4 week treatment, C57BL/6 mice were treated with the same concentrations of DBZ and MRK-560 but at a 5-day on/2-day off schedule. After treatment, thymus was isolated and single cells were prepared and stained for CD4, CD8, CD44 and CD25 to assess T cell development. To assess goblet cell hyperplasia, intestines from treated NSG mice were harvested and flushed with PBS and 10% neutral buffered formalin prior to fixation. For every mouse, a minimal of 10 villi were assessed for the number of secretory goblet cells. In addition, total body weight from all treated mice was assessed during and after treatment.

Immunohistochemistry. Tissues were collected and fixed in 10% neutral buffered formalin (Sigma) for 48 hours and then processed for paraffin embedding (HistoStar™ Embedding Workstation). Sections of 7 μm of thickness obtained from the paraffin-embedded tissues (Thermo Scientific Microm HM355S microtome) were mounted on Superfrost™ Ultra Plus™ Adhesion slides (Thermo Scientific) and routinely stained with hematoxylin and eosin (Mayers Haematoxylin 1l, Leica, 3801582E and Eosin Y solution, aqueous (1 liter), Sigma-Aldrich, HT110232-1L) for histopathological examination. Sections were then stained with periodic acid–Schiff (PAS): Slides were incubated in freshly prepared periodic acid (0.5 %) for 15 min and rinsed and incubated for another 5 min in distilled water. The Schiff reagent (Sigma-Aldrich, 3952016-500ML) was added onto the slides and kept for 15 min at room temperature in dark. The sections were then washed in slightly lukewarm running tap water for 5 min, rinsed and incubated in distilled water for 2 min, and counterstained in Mayer's hematoxylin (Mayers Haematoxylin 1l, Leica, 3801582E) for 1 min. After washing in running tap water for 5 min sections were dehydrated (95% EtOH, 100% EtOH, 100% EtOH, 3 min each, followed by two times xyleen for 5 min) and mounted in DPX mounting medium (Sigma, 06522). Images were acquired on the Zeiss Axio Scan.Z1 using an x20 objective and ZEN 2 software. For exporting images the ZEN 2 software (Zeiss) was used.

Immunofluorescence with tyramide signal amplification. Following antibodies were used for detecting the respective proteins: anti-Ki67 (rabbit, 1:1000, ThermoScientific, RM-9106-S, Clone SP6), anti-HLA-A (rabbit, 1:1250, Abcam, ab52922). Furthermore, the PerkinElmer Opal 4-Color Manual IHC Kit (PerkinElmer, NEL810001KT) was used for the tyramide signal amplification according to the manufacturer's protocol. For introduction of the secondary-HRP the Envision+/HRP goat anti-Rabbit (Dako Envision+ Single Reagents, HRP, Rabbit, Code K4003) was used for antibodies raised in rabbit. The various proteins were detected using the OPAL 520 for ki67 and OPAL 690 for HLA-A. Images were acquired on the Zeiss Axio Scan.Z1 using a x20 objective and ZEN 2 software. For exporting

images the ZEN 2 software (Zeiss) and the software package QuPath Version: 0.1.2 was used (*(68); https://github.com/qupath/qupath/wiki/Citing-QuPath)*. QuPath was also used for automatic cell detection using the DAPI channel and for subsequent creation of a detection classifier using all 55 given parameters resulting in the classification of Ki67 and HLA-A-double positive cells within the subpopulation of all HLA-A positive cells in the whole slide.

Flow cytometric analysis of hematopoietic populations. Single-cell suspensions were prepared from peripheral blood, bone marrow, spleen, thymus and lymph nodes. Single cells were stained with antibodies against CD4-eFluor 450 (eBioscience), CD4-PECy7 (eBioscience) or CD4-PE (eBioscience), CD8-PerCp-eFluor 710 (eBioscience), CD8-APC-eFluor 780 (eBioscience) or CD8-APC (eBioscience), CD25-Alexa-488 (eBioscience) or CD25-APC (BD Pharmingen), CD44-Brilliant Violet 510 (Biolegend) or CD44-PerCpCy5 (eBioscience) and hCD45-APC (eBioscience), as indicated and analyzed on a FACSCanto flow cytometer (BD Biosciences) or a MACSQuant VYB cell cytometer (Miltenyl Biotec). Data were analyzed using FlowJo software (Tree star).

Quantitative real-time PCR. RNA was extracted from tissue and cells using the illustra RNAspin Mini Kit (GE Healthcare Life Sciences) as per manufacturer's instructions. cDNA synthesis was carried out using GoScript (Promega) and real time quantitative performed using the GoTaq qPCR master mix (Promega) with the ViiA7 Real Time PCR system (Applied Biosystem). Quality control, primer efficiency and data analysis carried out using qbase+ software (Biogazelle). All gene expression was normalized using two housekeeping reference genes. Primers used for qPCR are listed in Supplementary Table S1.

Proliferation assays and cell cycle analysis. T-ALL cell lines HPB-ALL, DND-41 and Jurkat were treated with the γ-secretase inhibitors DAPT and MRK-560 as indicated for 14 days. Cells were subcultured every 2-3 days by centrifugation and resuspension in fresh medium containing indicated compounds, as described previously *(39)*. Total cell numbers and cell viability were determined by measuring FSC/SSC on a MACSQuant VYB cell cytometer (Miltenyl Biotec). Cell cycle assays were performed with the Click-iT™ Plus EdU Alexa Fluor™ 488 Flow Cytometry Assay Kit (Thermofisher scientific) as per manufacturer's instructions. Briefly, 400 000 cells/ml were seeded, and treated with DMSO, 100, 300 and 1000nM MRK-560 for 5 days. Two hours before the indicated time point, the cells were pulsed with 10 μM EdU. Cells were collected, washed and fixed. The FxCycle™ Violet Ready Flow™ DNA stain (Thermofisher scientific) was added, followed by 30 min incubation time. Stained cells were analysed on the MACSQuant Vyb (Miltenyi). Data analysis was performed using FlowJo software (Tree Star).

Fig. S1

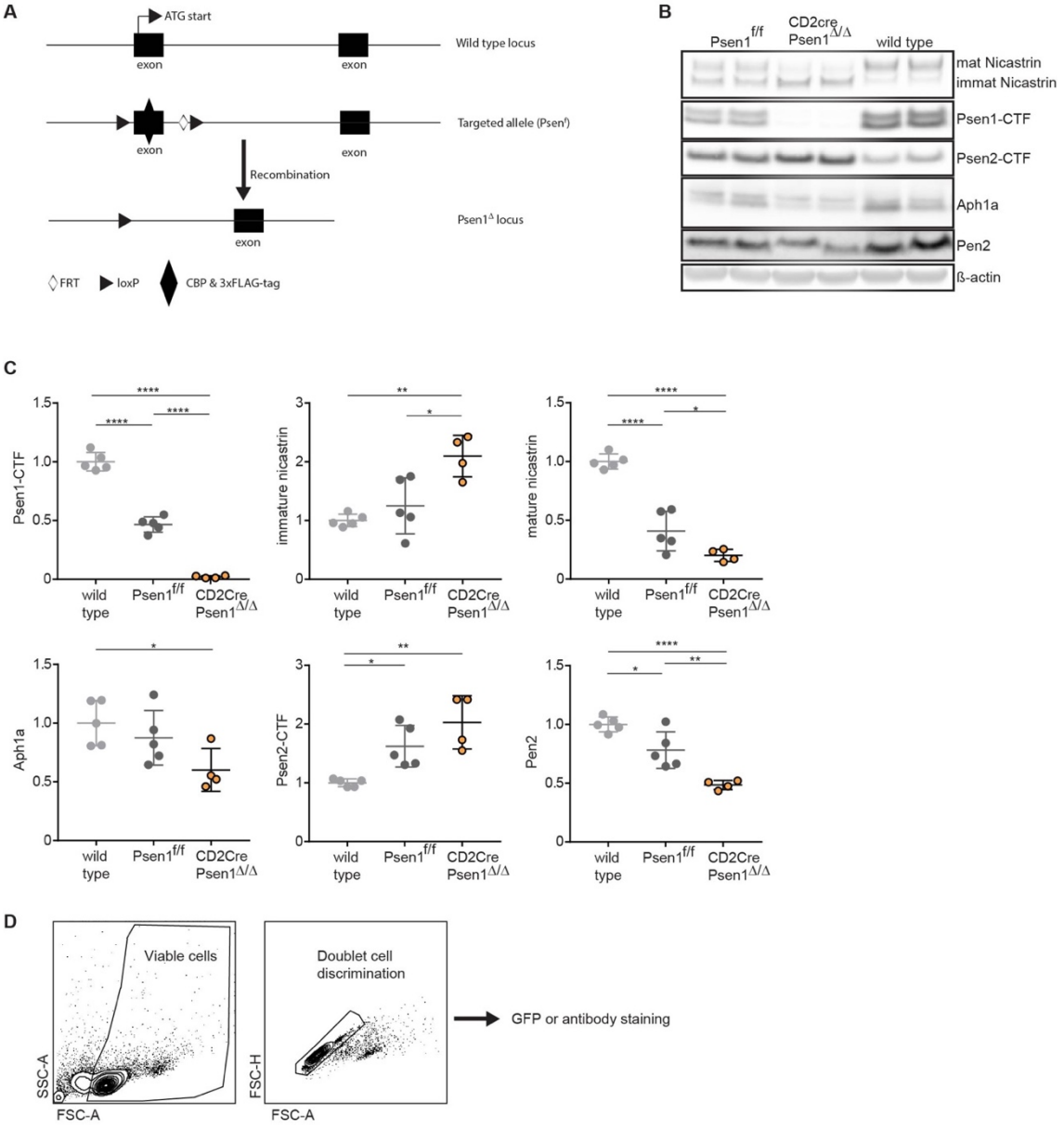

Fig. S1. Psen1 deletion does not affect T-cell development.

(**A**) Generation of Psen1 conditional knockout mice. (**B**) Representative western blot analysis of total thymus of C57BL/6 wildtype, $Psen1^{f/f}$ or $CD2CrePsen1^{\Delta/\Delta}$ mice for the different gamma-secretase subunits, Nicastrin, Psen1, Psen2, Aph1a, Pen2 and β-actin. (**C**) Quantification of protein levels of gamma-secretase subunits from **B**. (**D**) Gating strategy used for all flow-cytometry plots depicted in the manuscript. First, cells were gated according to physical parameters (FSC-A/SSC-A) in order to discard cell-debris and residual red blood cells. Next, cell singlets were gated (FSC-A/FSC-H) to discard clumps and doublets. These populations were then either assessed for GFP-levels or stained with the appropriate antibodies as described. All graphs show the mean values, error bars represent standard deviation. P values in **C** were calculated using one-way ANOVA. * $P \leq 0.05$, ** $P \leq 0.01$ and **** $P \leq 0.0001$.

Fig. S2

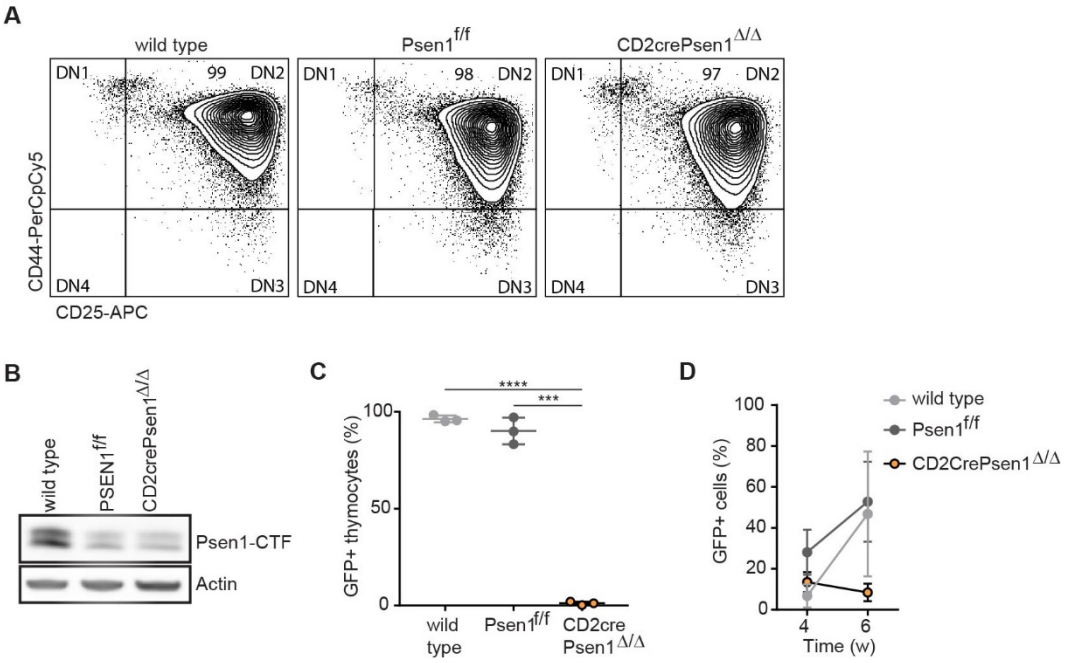

Fig. S2. Psen1 deletion does not affect engraftment in bone marrow transplants.

(**A**) Representative flow-cytometry plots of ex vivo cultures of mouse pro-T cells derived from C57BL/6 wild type, Psen1$^{f/f}$ or CD2CrePsen1$^{\Delta/\Delta}$ mice stained with antibodies to CD44 and CD25. (**B**) Western blot analysis for Psen1 and β-actin of enriched hematopoietic stem and progenitor cells isolated from C57BL/6 wildtype, Psen1$^{f/f}$ or CD2CrePsen1$^{\Delta/\Delta}$ donor mice used for transplantation. (**C**) Quantification of GFP^{+} cells in thymi from mice transplanted with wildtype, Psen1$^{f/f}$ or CD2CrePsen1$^{\Delta/\Delta}$ progenitors expressing ΔEGF-NOTCH1-L1601P-ΔP 9 weeks after transplant. (**D**) Quantification of levels of circulating GFP^{+} cells in peripheral blood from mice transplanted with wildtype, Psen1$^{f/f}$ or CD2CrePsen1$^{\Delta/\Delta}$ progenitors expressing ΔEGF-NOTCH1-L1601P-ΔP 4 and 6 weeks after transplant. All graphs show the mean values, error bars represent standard deviation. The P values in **C** were calculated using one-way ANOVA. *** $P \leq 0.001$ and **** $P \leq 0.0001$.

Fig. S3

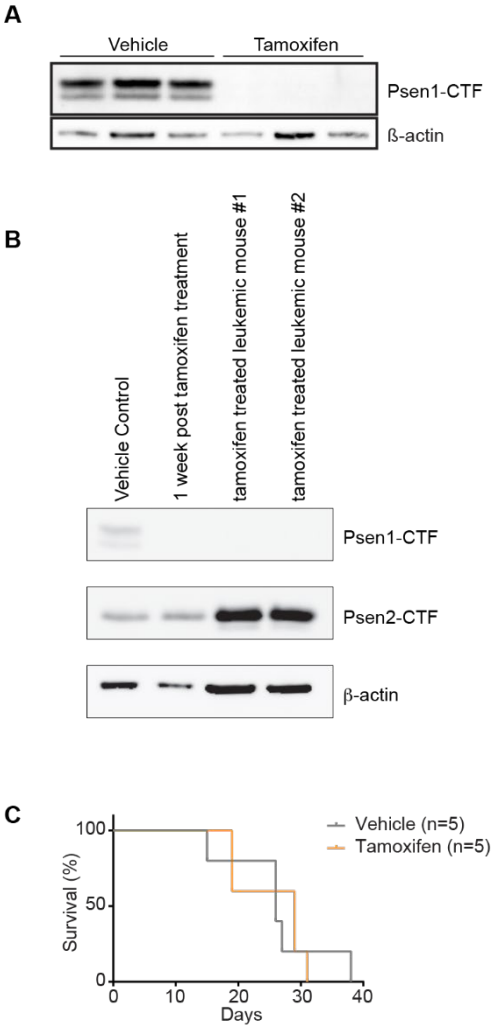

Fig. S3. Tamoxifen does not affect leukemia progression.

(**A**) Western blot analysis for Psen1 and β-actin in leukemic cells recovered from spleens ~2 weeks post-tamoxifen or vehicle treatment from mice transplanted with R26Cre-ER^{T2}Psen1$^{f/f}$ progenitors expressing ΔEGF-NOTCH1-L1601P-ΔP. (**B**) Western blot analysis for Psen1, Psen2 and β-actin in leukemic cells recovered from a vehicle treated spleen, or spleens after ~1 week post-tamoxifen treatment and two mice that developed leukemia after tamoxifen treatment in mice transplanted with R26Cre-ER^{T2}Psen1$^{f/f}$ progenitors expressing ΔEGF-NOTCH1-L1601P-ΔP. (**C**) Kaplan-Meier survival curves of mice transplanted with C57BL/6 wildtype progenitors expressing ΔEGF-NOTCH1-L1601P-ΔP treated either with vehicle or tamoxifen (100 mg/kg/day tamoxifen by I.P. injection on 5 consecutive days). All graphs show the mean values, error bars represent standard deviation. The P values in **C** were calculated using the log-rank test.

Fig. S4

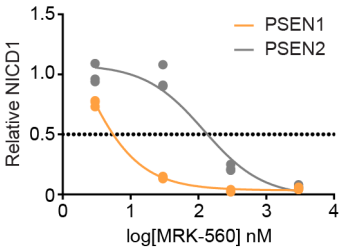

Fig. S4. MRK-560 shows selectivity for PSEN1 over PSEN2.

Quantification of NICD1 generation in MEFs expressing PSEN1 or PSEN2 γ-secretase complexes in response to MRK-560 treatment (n=3).

Fig. S5

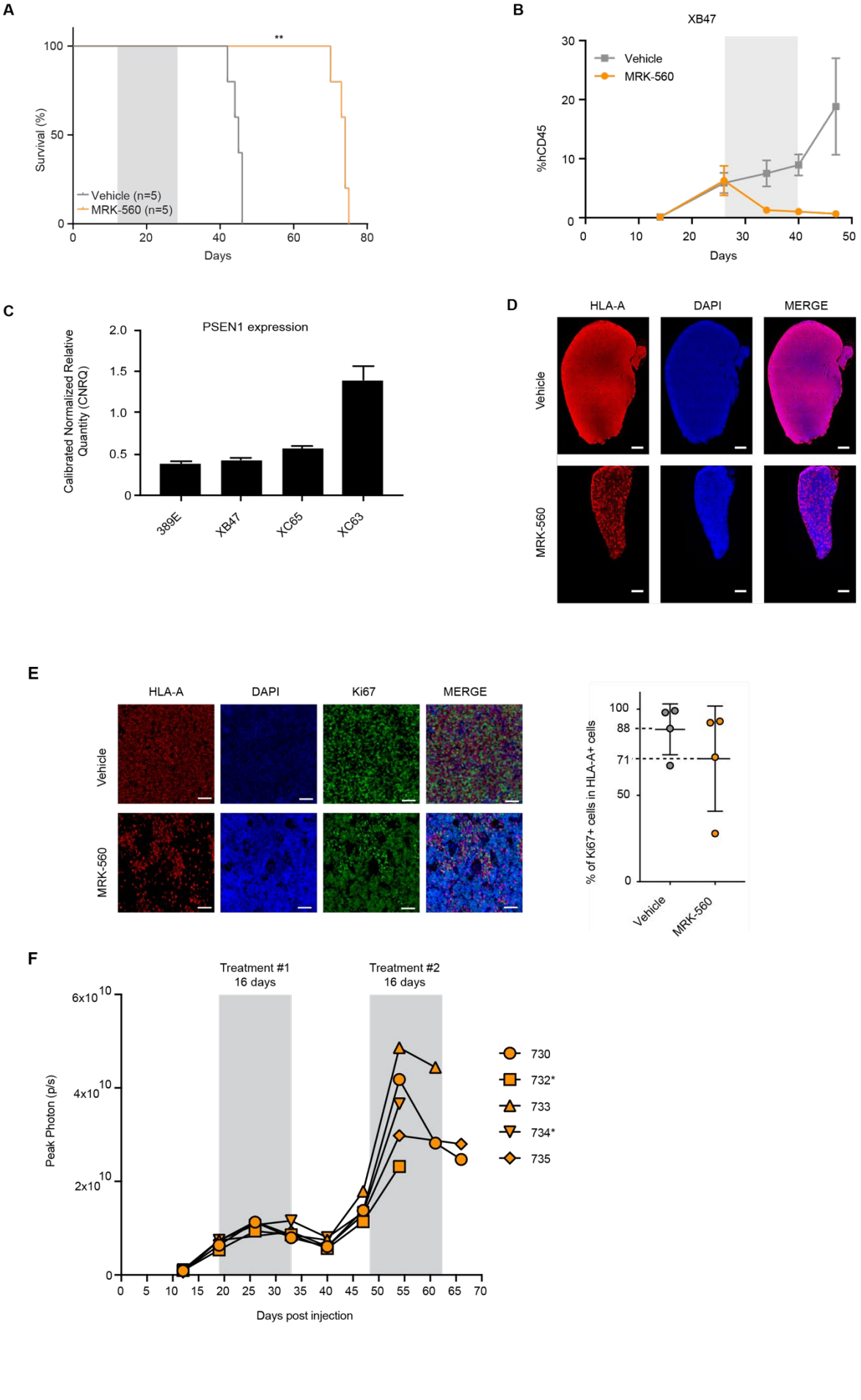
A
Survival (%)
Days
Vehicle (n=5)
MRK-560 (n=5)
**
B
XB47
Vehicle
MRK-560
%hCD45
Days
C
PSEN1 expression
Calibrated Normalized Relative Quantity (CNRQ)
389E
XB47
XC65
XC63
D
HLA-A
DAPI
MERGE
Vehicle
MRK-560
E
HLA-A
DAPI
Ki67
MERGE
Vehicle
MRK-560
% of Ki67+ cells in HLA-A+ cells
F
Treatment #1
16 days
Treatment #2
16 days
Peak Photon (p/s)
Days post injection
730
732*
733
734*
735

Fig. S5. Treatment of patient derived xenograft samples with MRK-560.

(A) Kaplan-Meier survival curves of mice transplanted with patient sample XC65 treated with vehicle or MRK-560 for 14 days. Treatment was started when 1% hCD45+ cells were detected in the blood. **(B)** Leukemia burden assessed by human CD45 staining of peripheral blood following 14 days treatment with 30 µmol/kg MRK-560 or vehicle by subcutaneous injection (grey box) of PDX XB47. **(C)** quantitative real time PCR analysis of PSEN1 levels. **(D)** Human HLA-A immunofluorescent staining of spleen sections from PDX XC63 taken immediately following 14 days treatment with 30 µmol/kg MRK-560 or vehicle by subcutaneous injection (Scale bar = 500 µm). **(E)** Representative higher magnification of Human HLA-A and Ki67 immunofluorescent staining of spleen sections from PDX XC63 taken immediately following 14 days treatment with 30 µmol/kg MRK-560 or vehicle by subcutaneous injection. Associated quantification of Ki67 in HLA-A positive cells comparing MRK-560 (n=4) and Vehicle (n=4) treated mice (Scale bar = 50 µm). **(F)** Leukemia burden assessed by bioluminescence after two rounds of 30 µmol/kg MRK-560 treatment of PDX XC65, with second round of treatment begun during relapse to determine if sensitivity is maintained to MRK-560.

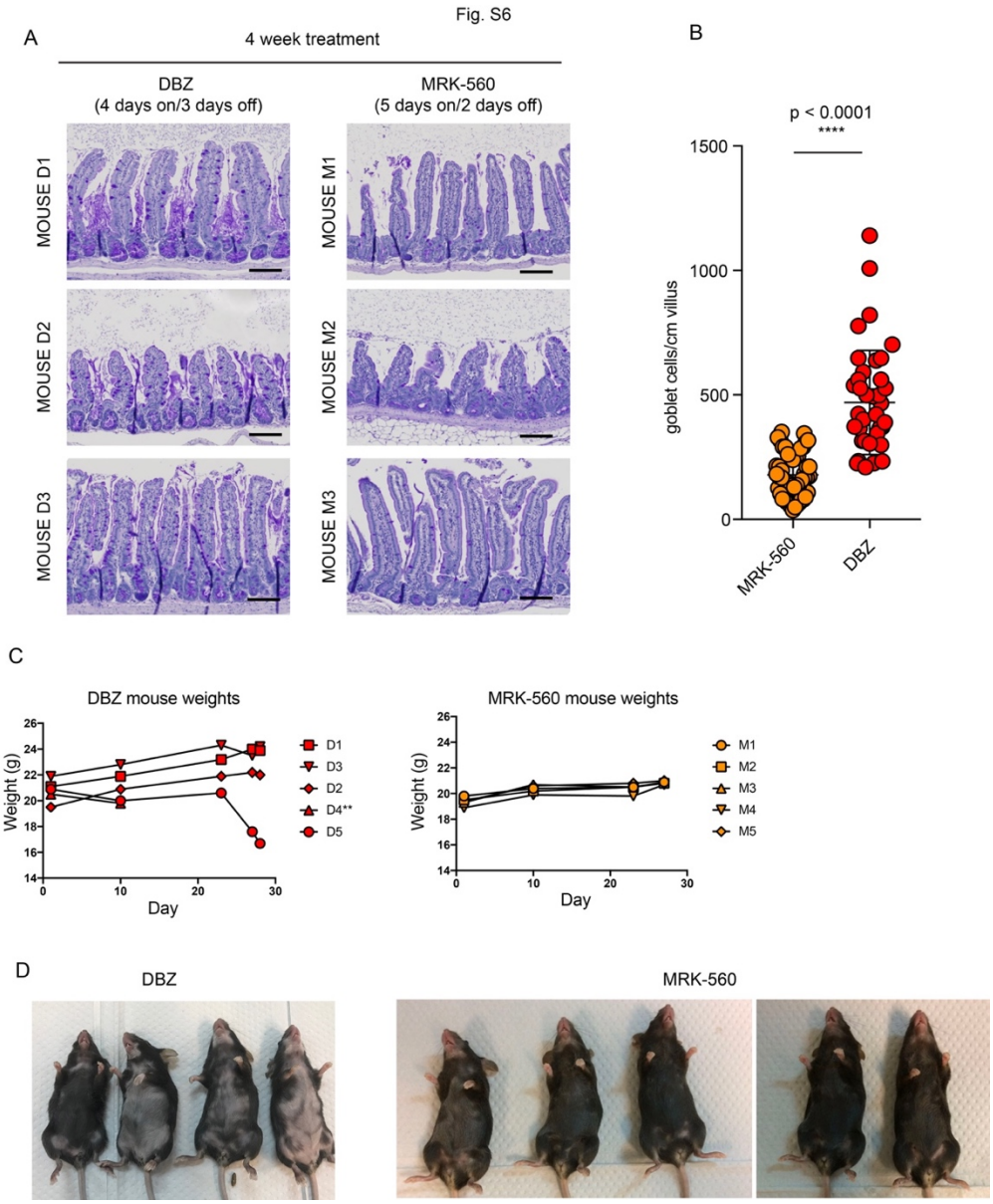

Fig. S6. Long term treatment with MRK-560 leads to significantly less gastrointestinal toxicity compared to DBZ.

(A) Representative images of Periodic Acid-Schiff staining of intestines from mice treated with MRK-560 or the broad-spectrum γ-secretase inhibitor Dibenzazepine (DBZ) for 4 weeks to assess the number of secretory goblet cells. Scale bars represent 100 μm. **(B)** Quantification of the number of goblet cells per cm villus with 10 villi counted per mouse (MRK-560 n=5 and DBZ n=4, respectively). **(C)** Weights of mice over the 4 week treatment period**. (D)** Visible hair loss in DBZ treated mice compared to MRK-560 treated mice at end of 4 week treatment period.

Table S1. Primers used for qPCR.

Gene	Forward	Reverse
DTX1	CGCAAGACCAAGAAGAAGC	CTCATCAGGTGGGTTTTTCAC
MYC	CTCGGATTCTCTGCTCTCCT	TTTCCACAGAAACAACATCG
NOTCH3	TTACGACTGTGCCTGTCTTCC	TATAGGTGTTGACGCCATCC
HPRT	TGACACTGGCAAAACAATGCA	GGTCCTTTTCACCAGCAAGCT
TBP	CGGCTGTTTAACTTCGCTTC	CACACGCCAAGAAACAGTGA

Table S2. T-ALL cell lines and patient derived xenograft models.

	Mutations	**Subtype**
Cell lines		
HPB-ALL	*NOTCH1(L1575P), NOTCH1 PEST indel FBXW7(R347H), WT1(S189*), TP53(R141C)*	*TLX3*
DND-41	*NOTCH1(L1594P), NOTCH1(D1610V), NOTCH1 PEST indel, IL7R indel, NRAS(Q61H)*	*TLX3*
Jurkat	*PTEN deletion, TP53 R64*, NOTCH1 ins1740QAVEPPPPAQLHFMYVA*	*TAL1*
PDX samples		
XC63	*NOTCH1*(L1678P), NOTCH1(Q2459*), *JAK3*(M511I)	*immature*
XC65	*NOTCH1*(A2438fs*), *JAK1* (R724H)	*immature*
389E	*NOTCH1*(L1600P), NOTCH1(P2514fs*), *JAK3*(M511I), *DNM2*	*immature*
XB47	*NOTCH1(L1600P), NOTCH1(Y2490*), RPL10(R98S), CNOT3(R745ins), del(9)(p21p21)*	*TAL1*